TESE DE DOUTORADO

Seismic Amplitude Analysis and Quality Factor Estimation Based on Redatuming

FRANCISCO DE SOUZA OLIVEIRA

BELÉM-PARÁ

2015

FRANCISCO DE SOUZA OLIVEIRA

Seismic Amplitude Analysis and Quality Factor Estimation Based on Redatuming

Tese apresentada ao Programa de Pós-Graduação em Geofísica do Instituto de Geociências da Universidade Federal do Pará, em cumprimento às exigências para obtenção do título de Doutor em Geofísica.

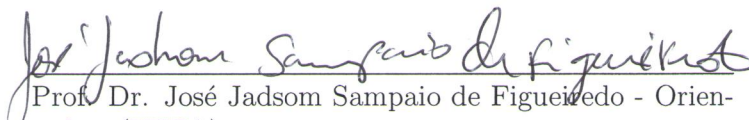Orientador: José Jadsom Sampaio de Figueiredo

FRANCISCO DE SOUZA OLIVEIRA

Seismic Amplitude Analysis and Quality Factor Estimation Based on Redatuming
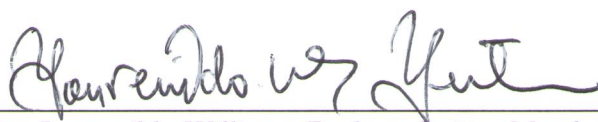
Tese de Doutorado Apresentada ao Programa de Pós-Graduação em Geofísica da Universidade Federal do Pará para Obtenção do Título de Doutor em Geofísica.

Data de aprovação: 25/04/2015

Conceito: BOM

Banca Examinadora:

Prof. Dr. José Jadsom Sampaio de Figueiredo - Orientador (UFPA)

Prof. Dr. Lourenildo Williame Barbosa Leite - Membro (UFPA)

Prof. Dr. João dos Santos Protázio - Membro (UFPA)

Prof. Dr. Amin Bassrei - Membro (UFBA)

Dr. Tiago Antonio Alves Coimbra - Membro (CEPETRO-UNICAMP)

A meus familiares e amigos.

AGRADECIMENTOS

Gostaria de agradecer a Deus que me sustentou e me guiou até aqui. Ao meu orientador o Professor Dr. José Jadsom Sampaio de Figueiredo pela dedicação, pela amizade compartilhada, pelas incontáveis horas dedicadas e pelas valiosas discursões que contribuiram para o desenvolvimento deste trabalho.
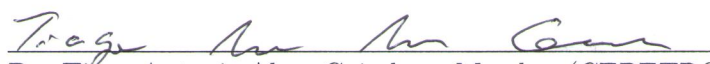
Reconheço e agradeço o indispensável apoio financeiro recebido do Centro de Apoio à Pesquisa (CAPES) e do Conselho Nacional de Desenvolvimento Científico e Tecnológico (CNPQ). Agradeço o National Snow & Ice Data Center pelo fornecimento dos dados de GPR e a Exxon Mobil pelo fornecimento dos dados reais sísmicos do Mar do Norte da Noruega (Viking Graben).

Agradeço aos membros da banca examinadora, pela disponibilidade e pelas contribuições apresentadas para o aperfeiçoamento deste trabalho.

Agradeço a Professora Dra. Maria Amélia Novais Schleicher e ao Professor Dr. Joerg Schleicher pela oportunidade de visita à Unicamp, que foi fundamental para o desenvolvimento deste trabalho.

Agradeço a coordenação do CPGF, na pessoa da Profa. Dra. Ellen de Nazaré Souza Gomes, pela oportunidade e pela confiança creditada. Aos funcionarios técnicos e administrativos do Instituto de Geociências, os Professores em especial a Profa. Dra. Midori Makino e o Prof. Dr. Hernani Brazão e as Secretarias do curso do CPGF Benildes Lopes e Lucibela Cardias, pela inestimada amizade, pela dedicação e carinho ao longo desses anos.

Aos Amigos da Unicamp Lucas Freitas, Tiago Coimbra e Rafael Aleixo, do CPGF Andrei Oliveira, Wildney Vieira, Rubenvaldo, Jaime Colazzos, Carolina Barros, Wilson Lopes e Paola Cardias pelas discurções valorosas e pelos incentivos ao longo dos anos.

Agradeço aos meus familiares Girllene Ramalho, Gustavo Ramalho, Ivanilde Oliveira, Alexandre Oliveira, Francisco Menezes, Geraldo Menezes, Aline Pinto e Sandra pelo apoio, paciência e compreensão pela ausência durante todos estes anos.

Por fim, presto meus agradecimentos à todos que colaboraram direta ou indiretamente para a concretização deste projeto, sem os quais, não seria possível a sua realização.

"No fim tudo dará certo, basta acreditar, confiar e trabalhar."

(Girllene Ramalho)

RESUMO

A correção de amplitude é uma tarefa importante para corrigir a dissipação de energia sísmica por espalhamento geometrico ou atenuação durante a propagação da onda acústica / elástica em sólidos. Neste trabalho, propomos uma forma de estimar o fator de qualidade dos dados de reflexão sísmica, com uma metodologia baseada na combinação do método de deslocamento da frequência de pico (PFS) e do operador de redatumação. A contribuição deste trabalho está em corrigir os tempos de trânsito quando o meio é formado por muitas camadas. Em outras palavras, a correção da tabela de tempo de trânsito utilizada no método PFS é realizada utilizando um operador de redatumação. A operação proposta, é realizada de forma iterativa, com isto, permitindo estimar o fator de qualidade Q, camada por camada de um modo mais preciso. A operação de redatumação é usada para simular a aquisição de dados em novos níveis, evitando distorções produzidas por irregularidade próximas da superfície relacionadas com a geometria ou com as propriedades de heterogeneidade do meio. Propomos uma aplicação do operador de redatumação Kirchhoff em verdadeira ampiltude (TAKR) em meios homogêneos e comparamos com o operador de redatumação Kirchhoff convencional (KR) restrito ao caso de afastamento nulo. Nossa metodologia é baseada na combinação do método de deslocamento da frequência de pico e o operador de redatumação (TAKR com peso igual a 1). Aplicação em dados sintéticos e em dados reais sísmico (Viking Graben) e GPR (Siple Dome) demonstra a viabilidade de nossa análise.

Palavras-chave: Redatumação Kirchhoff. Redatumação Kirchhoff em verdadeira ampiltude. Análise de amplitude. Análise de tempo de trânsito. Estimativa do fator de qualidade. Método PFS. Filtragem inversa Q.

ABSTRACT

Amplitude correction is an important task to correct the seismic energy dissipated due the ineslasticity absortion and the geometrical spreading during the acoustic/elastic wave propagation in solids. In this work, we propose a way to improve the estimation of quality factor from seismic reflection data, with a methodology to estimate de quality factor based on the combination of the peak frequency-shift (PFS) method and the redatuming operator. The innovation in this work is in the way we correct travel times when the medium is consisted by many layers. In other words, the correction of traveltime table used in the PFS method is performed using the redatuming operator. This operation, which is performed iteratively, allows to estimate the Q-factor layer by layer in a more accurate way. A redatuming operation is used to simulate the acquisition of data in new levels, avoiding distortions produced by near-surface irregularities related to either geometric or material property heterogeneities. In this work, the application of the true-amplitude Kirchhoff redatuming (TAKR) operator on homogeneous media is compared with conventional Kirchhoff redatuming (KR) operator restricted to the zero-offset case. Our methodology is based on the combination of the peak frequency-shift (PFS) method and the redatuming operator (TAKR with weight equal 1). Application in synthetic and in seismic (Viking Graben) and GPR (Siple Dome) real data demonstrates the feasibility of our analysis.

Keywords: Kirchhoff redatuming. True-amplitude Kirchhoff redatuming. Amplitude analysis. Travel-time analysis. Quality factor estimation. PFS method. Inverse Q filtering.

SUMMARY

1 INTRODUCTION

1.1 Motivation

When seismic waves propagate inside the earth, they suffer amplitude attenuation and dispersion due to the inelasticity and the heterogeneities of the medium (RICKER, 1953; FUTTERMAN, 1962; WHITE, 1983; KNEIB; SHAPIRO, 1995). Attenuation refers to the exponential decay of the wave amplitude with distance and dispersion is a variation of propagation velocity with frequency. Attenuation and dispersion can be caused by a variety of physical phenomena that can be divided broadly into elastic processes, where the total energy of the wavefield is conserved (scattering attenuation, geometric dispersion), and inelastic dissipation, where wave energy is converted into heat. Specifically concerning exploration geophysics, the inelastic attenuation and dispersion of body waves (P- and S-waves) are a result of the presence of fluids in the pore space of rocks (MÜLLER; GUREVICH; LEBEDEV, 2010).

Related to inelasticity attenuation, the estimation and compensation of the absorption of seismic waves is a fundamental task in seismic processing and interpretation. These operations are important because they allow the improvement of the high-frequency (resolution) of seismic images and consequently provides a better interpretation of the effects of AVO, obtaining also information on lithology, saturation, permeability and pore pressure (BEST; MCCANN; SOTHCOTT, 1994; CARCIONE; HELLE; PHAM, 2003; CARCIONE; PICOTTI, 2006).

Several methods have been developed for estimating the quality-factor from reflection and transmission data. Dasgupta and Clark (1998) adapted the classic spectral ratio method (BATH, 1974) for determining the seismic quality factor Q from conventional common midpoint (CMP) gathers. Tonn (1991), using different numerical methods (among them spectral modeling and spectral ratio (BATH, 1974)) estimated the quality factor Q from VSP (vertical seismic profile) data. Blias (2012) also modified the spectral ratio method (BATH, 1974) for Q determination from near-offset VSP data. (BRZOSTOWSKI; MCMECHAN, 1992) estimated attenuation with a tomographic technique that is based on fitting log spectra with a Q model. Nunes et al. (2011) performed a comparative study to estimate the Q factor using different approaches, including the PFS method (ZHANG; ULRYCH, 2002) analyzed in this work.

It is well known that beyond of inelastic attenuation, the wave field also suffer the amplitude decay due the geometrical spreading (SHERIFF; GELDART, 1995). There are several methods to correct the geometrical spreading. For the horizontally layered

medium, Ursin (1990) found out a exact expression for geometrical spreading as function of velocity of first layer and the offset. Afterwards, Schleicher, Hubral and Tygel (1993) uses the dual diffraction stack methodology to remove the geometrical spreading of primary reflections. Related to the anisotropic medium, Xu and Tsvankin (2006), Xu and Tsvankin (2007) proposed a methodology to compensate the geometrical spreading along a raypath (for wide-azimuth) in stratified azimuthally anisotropic media. Beyond of those methods to correct the geometrical spreading, there are other related to redatuming (BERRYHILL, 1984; PILA et al., 2014).

Wavefield redatuming is an operation that transforms seismic data based on the assumption of a new measurement surface. In other words, given a data set acquired on an initial surface, it generates a simulated data set as if it were measured on another surface. Among its applications, we have near-surface corrections (COX; SCHERRER; CHEN, 1999), OBC processing (DAN et al., 2011), dual-sensor streamer de-ghosting (KLüVER,), and multiple attenuation (WIGGINS, 1988). The wave-equation based redatuming operators are the most accurate ones. Over the years several approaches have been proposed: based on the Kirchhoff integral (BERRYHILL, 1984), using the phase-shift method (MARGRAVE G.; FERGUSON R., 1999) and based on the common-focus point (CFP) technology.

The redatuming operators are especially costly in the pre-stack domain in which most applications occur. Though the Kirchhoff method is rather straightforward and efficient, it is still expensive compared to static correction and requires an accurate interval velocity field above the datum. In addition, the Kirchhoff scheme is applied to common source and receiver gathers; in other to relocate sources and receivers, respectively. An analytical Kirchhoff-type redatuming operator, based on straight ray approximation (SRD) (ALKHALIFAH; BAGAINI, 2006) fills the gaps between static correction and wave-equation re datuming. It uses the assumption of local homogeneity, potentially useful for most media. The small size of the operator and its analytical expression provides cost-effectiveness and little sensitivity to velocity errors. Toward a true-amplitude Kirchhoff-type operator, particular cases of the migration to zero-offset (MZO) operator proposed by Tygel et al. (1998) were analytically formulated for zero-offset configuration on homogeneous models and compiled into a true-amplitude Kirchhoff redatuming (TAKR) operator (PILA et al., 2014; OLIVEIRA; FIGUEIREDO; FREITAS, 2015).

This operator provides correct kinematic and dynamic redatumed traces. The reader should notice that the term true-amplitude is used here on a more strict sense, beyond amplitude relativity preservation. More specifically, the amplitude is not only preserved within a given event for different offsets. In this case, the amplitude has its geometrical spreading component adjusted to honor the new measurement surface. For seismic data processing, the restriction to zero-offset configuration limits the appli-

cability of a redatuming operator to event repositioning (e.g., in moving a stack from floating to final datum). However, as described by Liu, Lane and Quan (1998), zero-offset redatuming plays a more important role in imaging GRP profiles. Moreover, an amplitude-friendly processing sequence is of great importance since amplitude analysis of GPR profiles has applications in shallow aquifers characterization (BRADFORD, 1999), determination of subsurface contaminant (SCHMALZ; LENNARTZ, 2002) and soil water content variations (CASSIDY, 2007) in hydrological studies, and archaeological prospection (KHWANMUANG; UDPHUAY, 2012; ZHAO et al., 2013).

1.2 Objectives and disposition of thesis' chapter

In this thesis, in first point of view, we analyze the amplitude behavior of two Kirchhoff-based redatuming operators (KR and TAKR) through homogeneous media for the zero-offset case: the operator described by Berryhill (1984) and the true-amplitude operator proposed by Pila et al. (2014).

In a second point, here we combined the PFS method developed by Zhang and Ulrych (2002) with the redatuming operator (SCHNEIDER, 1978; PILA et al., 2014) in order to improve the estimative of the Q-factor from seismic surface data. In our approach, the redatuming operator plays an important role on correcting the approximation of the straight ray considered by Zhang and Ulrych (2002). In the dynamic point of view, the redatuming operator has been developed to recover true-amplitude (geometrical spreading correction) in the zero-offset domain (SCHNEIDER, 1978; PILA et al., 2014; OLIVEIRA; FIGUEIREDO; FREITAS, 2015). In this work only used this operator in the kinematic context, that does not show any limitation related to the type of offset.

In this thesis, additionally to the introductory chapter (Chapter 1), contains three chapters. In Chapter 2 presents a review of the theoretical development of operator redatuming analysis as it application on quality factor estimation through frequency-shift method (ZHANG; ULRYCH, 2002). In the sequence, in the Chapter 3, we presents the results of our analysis for a couple of numerical examples (for redatuming operator analysis and quality factor estimation), application in a real GPR dataset (in case of redatuming operator analysis) and in a real seismic data from Viking Graben field (quality factor estimation). Finally, Chapter 4 presents the conclusions about our analysis and interpretation.

2 THEORETICAL BACKGROUND

In this chapter we show an mathematical analysis for amplitude and travel-time attributes for the redatuming operation. This analysis relies on the stationary phase method to analytically solve the Kirchhoff redatuming in 2.5 D homogeneous media restricted to a zero-offset configuration. Beyond that, in the next stage we describe our methodology which is based on the combination of FPS method (ZHANG; ULRYCH, 2002) and redatuming operator (PILA et al., 2014; OLIVEIRA; FIGUEIREDO; FREITAS, 2015).

The corresponding processing sequence we uses the redatuming iteratively to obtain the correct traveltime arrival, and then in the subsequent step uses the FPS method to perform the estimative of quality factors.

2.1 Homogeneous Media With Topography

The redatuming is one of imaging operations that can be described by a chaining of Kirchhoff integrals of migration and demigration. For this purpose, it is necessary to carry out the exchange in the order of integrations and analytically evaluate the new inner integral. In this way, many imaging operators in a single step of type diffraction stacking can be developed (SCHLEICHER; M.; HUBRAL, 2007). In this study, we studied a true amplitude redatuming in 2,5-D, i.e., we study the behavior of the amplitude when the data is redatumed. The 2,5-D attribute (BLEISTEIN, 1986) indicates that in our experiments we consider a 3-D wave propagation in a medium with cylindrical symmetry, with the seismic survey perpendicular to the axis of symmetry. In this work, the speed is invariant in the direction y and the seismic line is positioned along the x axis.

In our experiment we consider a zero offset acquisition configuration, with receptor-sources equally spaced along the x axis. We also believe that all sources points and receptors are reproducible, meaning they have identical characteristics regardless of their current position. In the following analysis, the location of the positions of the sources and receivers along the original seismic line in Z_i acquisition on surface described by its horizontal coordinate ξ_i. In other words, the original positions of the sources S_i and G_i receptors are located in points $G = S = (\xi, 0, Z_o(\xi))$. Correspondingly, the positions of the simulated sources and receivers in the new datum Z_o are described by their horizontal coordinates η, i.e., they are located in points $G_o = S_o = (\eta, 0, Z_o(\xi))$.

We know that for every point (ξ, τ) to be built in redatumada section with tau the time in a new level or redatumed time, there is an operator diffraction weighted stacking along a stacking surface of the specific problem, the so-called inplanats $t = t_{red}(\xi; \eta, \tau)$,

which leads to the desired transformation real amplitude. Consequently, the simulated data at a new level can be expressed as a single operator with stacking weighting function $W_{red}(\xi; \eta, \tau)$ acting on the input data, i.e.,

$$U_o(\eta, \tau) = \frac{1}{\sqrt{2\pi}} \int_A d\xi \, W_red(\xi; \eta, \tau) \partial^{1/2} [U(\xi, t)]|_{t=\mathcal{T}_{red}(\xi; \eta, \tau)} , \qquad (2.1)$$

where $U(\xi, t)$ means the input data and $U_o(\xi, \tau)$ is the redatumed data. Also, A represents the opening of the stacking, which is the region over which the data is stacked to contribute to the output value at position (η, τ). Finally, $\partial^{1/2}$ is the half derivative of operation that helps to recover the pulse shape. It can be represented as

$$D^{1/2}[f(t)]| = \mathcal{F}^{-1} \left[|\omega|^{\frac{1}{2}} e^{-i\frac{\pi}{2} sign(\omega)} \mathcal{F}[f(t)] \right], \qquad (2.2)$$

where $\mathcal{F}$ is the Fourier transform.

Figure 2.1 – Schematic representation of redatuming $\mathcal{Z}_i$ acquisition surface and $\mathcal{Z}_o$ redatuming surface.
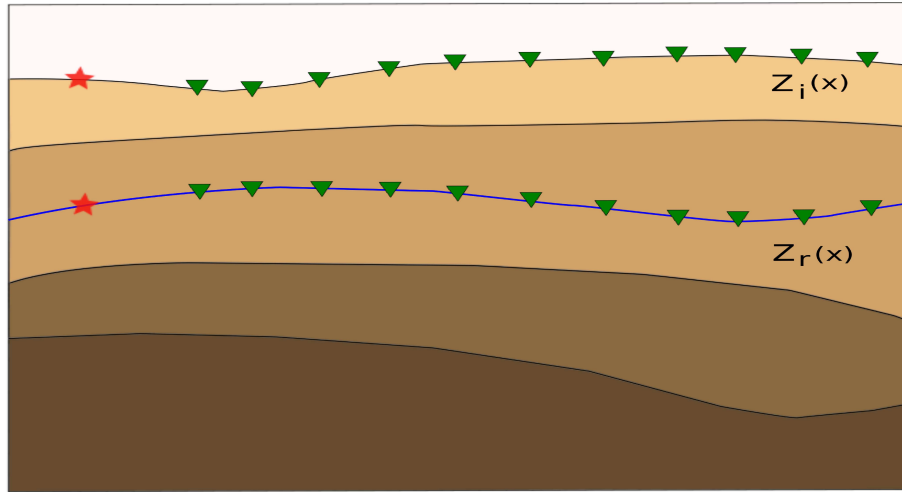
Source: From author

The determination of the stacking curve is related the kinematic properties of the problem. Stacking curve connects all the points in the input section, where the reflection event should have been recorded and should appear in redatumed section at the exit point (η, τ). On the other hand, the weighting function is related to the behavior of the amplitude. The condition for the weight function recover the amplitude is, asymptotically, the simulated reflection has the same geometrical spreading factor that reflections recorded in new datum. As shown by Pila et al. (2014), the resulting true amplitude weight function is independent of reflector properties, the weight function in a point (η, τ) depends solely on the velocity model v_o.

2.2   Diffraction Stacking and Weight Function

Pila et al. (2014) showed how the stacking line and the weight function should be modified if the topography is present on the surface of acquisition $zi = (\xi)$ and the new datum $z_o = (\eta)$. The stacking curve

$$\mathcal{T}_{red}(\xi; \eta, \tau) = \frac{2}{v_o}(R_o + \alpha) = \tau + 2\frac{\alpha}{v_o}. \tag{2.3}$$

is still valid, with α representing the distance between S_i and S_o. For this reason the calculations to obtain the weight function are possible using geometric arguments. Given a point (η, τ) in the output section, have their isochronous is represented by the following semi-circle

Figure 2.2 – The single ray coming out of a pair of source and receiver input for the isochronous $z = Z_o(\xi, \eta, \tau)$ through the center of the semicircular isochronous, and back to the same place.
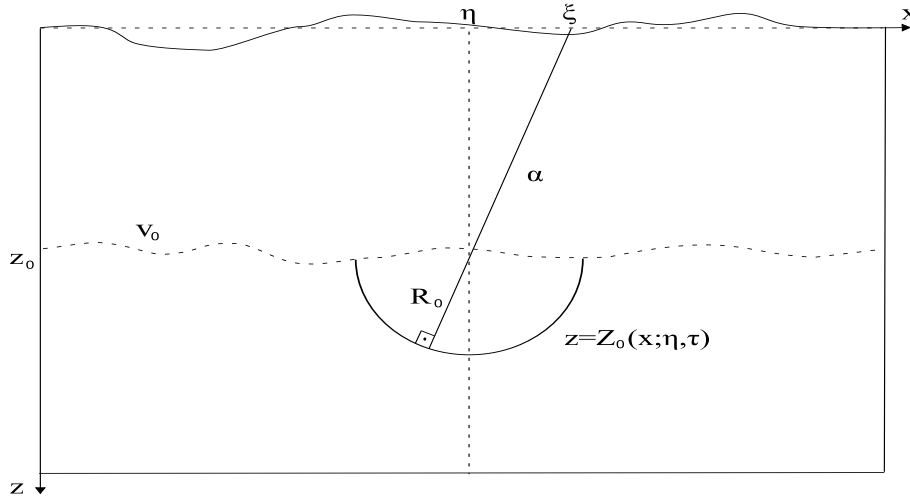
Source: From author

$$z = \mathcal{Z}_o(x; \eta, \tau) = z_o(\eta) + \sqrt{R_o^2 - (x - \eta)^2}. \tag{2.4}$$

The reflections that matter are those orthogonal the isochronous 2.4. So to Figure 2.2 we see that given a ξ, the only ray that part of the source-receiver pair and back to the same place, is the one passing through the center of isochronous Z_o because the reflection must be orthogonal to this curve. This beam travels a distance of $2(R_o + \alpha)$ until the receiver, with $R_o = \frac{v\tau}{2}$. Therefore, the redatumed time of isochronous 2.4 in the input section is given by 2.3 and the stationary point where this reflection occurs is defined by

$$x^* = \frac{\gamma R_o}{\alpha} + \eta, \tag{2.5}$$

where now due to topography have that $\gamma = \eta - \xi$ and $\alpha = \sqrt{\gamma^2 + [z_o(\eta) - z_i(\xi)]^2}$. Then determine the curvatures of isochronous. Making use of isochronous input section now includes information regarding the topography and is represented by the equation

$$z = \mathcal{Z}_i(x; \xi, \tau) = z_i(\xi) + \sqrt{(v_o t/2)^2 - (x - \xi)^2}. \tag{2.6}$$

So the curvatures of isochronous 2.4 and 2.6, on the stationary point are given by

$$K_o = -\frac{1}{R_o} \tag{2.7}$$

and

$$K_i = -\frac{1}{(R_o + \alpha)}. \tag{2.8}$$

To finalize the terms of optical length $\sigma_{iS} = v_o(R_o + \alpha)$, $\sigma_{iG} = v_o R_o$ and geometrical spreading $\bar{L}_{oS} = R_o/v_o$. The latter term being determined for the calculation of the weight function and angle θ_S^* of segment M_S^* (PILA et al., 2014). Due to the presence of the topography on the surface, this angle is not equal to the angle of propagation θ. Now $\theta^* = \theta_S^* + \phi$ where ϕ is the angle that the normal to the surface of S_i makes with the vertical, i.e., $tan\phi = z_i'(\xi)$. Where $cos\theta_S^* = cos(\theta^* - \phi)$, thus

$$\cos \theta_S^* = \cos \phi \left[z_o(\eta) - z_i(\xi) - \gamma z_i'(\xi) \right] / \alpha. \tag{2.9}$$

Thus realizing the necessary replacements on the equation of weight function to a zero-offset configuration (PILA et al., 2014), the equation reduces to

$$W_{red}(\xi_i, \eta, \tau) = \sqrt{\frac{1}{v_o} \left(\frac{R_o + \alpha}{R_o} \right)} \frac{[z_o(\eta) - z_i(\xi) - \gamma z_i'(\xi)]}{\alpha^{3/2}}. \tag{2.10}$$

The weight function without geometrical spreading correction is called in this work of the weight to preserve the amplitude and it is defined by

$$W_{pa}(\xi_i, \eta, \tau) = \sqrt{\frac{1}{v_o}} \frac{[z_o(\eta) - z_i(\xi) - \gamma z_i'(\xi)]}{\alpha^{3/2}}. \tag{2.11}$$

The weight function W_{red} in the next section will be renamed to W_{ta} (weight in true amplitude) and the distance α will be represented by d.

2.3   2.5 D Kirchhoff-Based Redatuming

Kirchhoff redatuming is based on the integral formulation of Kirchhoff migration (SCHNEIDER, 1978). Like its migration counterpart, the redatumed wavefield U_o is calculated by successive weighted summations of input wavefield U_i along proper trajectories. More specifically,

$$U_o(\xi_o, t_o) = \frac{1}{\sqrt{2\pi}} \int_{Z_i} W(\xi_i, \xi_o, \tau) \partial^{1/2} U_i(\xi_i, t \pm \tau) d\xi_i, \tag{2.12}$$

where ξ_i and ξ_o are the horizontal coordinates of the input and output datums Z_i and Z_o, $\partial^{1/2}$ denotes the half-derivative, τ is the traveltime between the output location $(\xi_o, Z_o(\xi_o))$ and input location $(\xi_i, Z_i(\xi_i))$, $W(\xi_i, \xi_o, \tau)$ is a properly chosen weight. In frequency domain the $\partial^{1/2}$ corresponds to $\sqrt{i\omega}$. Note that the $\pm$ sign is chosen appropriately whether the output datum is above $(-)$ or below $(+)$ the input datum.

We analyse the amplitude behavior of two Kirchhoff-based redatuming operators through homogeneous media for the zero-offset case: the preserving operator described by Berryhill (1984), and the true-amplitude operator proposed by Pila et al. (2014).

These operators are kinematically identical. As expected, when redatuming from datum Z_i to Z_o, through a homogeneous media with velocity v, the travel-time τ is directly calculated for the distance between input and output locations $d(\xi_i, \xi_o)$, namely the weight function W_{pa} (Equation 2.11) can be rearranged becomes

$$W_{pa}(\xi_i, \xi_o, \tau) = \sqrt{\frac{1}{v}} \frac{[z_o(\xi_o) - z_i(\xi_i) - \gamma z_i'(\xi_i)]}{d^{3/2}}, \tag{2.13}$$

$$W_{pa}(\xi_i, \xi_o, \tau) = \sqrt{\frac{1}{vd}} \frac{[z_o(\xi_o) - z_i(\xi_i) - \gamma z_i'(\xi_i)]}{d}, \tag{2.14}$$

$$W_{pa}(\xi_i, \xi_o, \tau) = \frac{\phi(\xi_i, \xi_o)}{\sqrt{vd}}, \tag{2.15}$$

where

$$\phi(\xi_i, \xi_o) = d^{-1} \left[Z_o(\xi_o) - Z_i(\xi_i) - (\xi_o - \xi_i) Z_i'(\xi_i) \right] \tag{2.16}$$

accounts for the incidence correction. On the other hand, the true-amplitudes corrections are obtained incorporating a geometrical spreading adjusting term

$$W_{ta}(\xi_i, \xi_o, \tau) = \frac{R_o + d}{R_o} \frac{\phi(\xi_i, \xi_o)}{\sqrt{vd}}, \tag{2.17}$$

or

$$W_{ta}(\xi_i, \xi_o, \tau) = (1 + \frac{d}{R_o}) \frac{\phi(\xi_i, \xi_o)}{\sqrt{vd}}, \tag{2.18}$$

then we can conclude that the geometrical spreading term is given by

$$\mathcal{G}(\xi_i, \xi_o, t_o, v) = (\frac{2d}{vt_o}), \tag{2.19}$$

into the summation weights, generating the true-amplitude weight W_{ta} given by

$$W_{ta}(\xi_i, \xi_o, \tau) = (1 \pm \mathcal{G}) W_{pa}$$

$$= \left(1 \pm \frac{2d}{vt_o}\right) \frac{\phi(\xi_i, \xi_o)}{\sqrt{vd}}. \tag{2.20}$$

where t_0 is the output time and d is the distance between input and output locations.

2.3.1 Analytical analysis of velocity sensitiveness

A first understanding of the impact of velocity errors on both operators (KR and TAKR) can be obtained by analytical analysis of a simple case. In order to achieve that, we derive the stationary phase approximation (BLEISTEIN, 1984) of equation 2.1 in frequency domain (see Appendix A) in the case of horizontal plane input and output datums and reflector and constant velocity. The stationary phase method equation is defined by

$$U_o(\xi_o, \omega) \approx \sqrt{\frac{2\pi}{i\omega\phi''(\xi_o; \xi_o)}} U_i(\xi_i, \omega) e^{i\omega\phi(\xi_i;\xi_o)+i\pi/4sgn(\sigma)sgn(\phi''(\xi_i;\xi_o))}. \tag{2.21}$$

In the case of a reflector located at depth D and with unitary reflectivity, the zero-offset input dataset $U_i(\xi_i, t)$ is given in frequency domain by

$$U_i(\xi_i, \omega) = \frac{1}{4\pi D} e^{-i\omega 2D/v}, \tag{2.22}$$

where v is the medium velocity. Therefore, when using a redatuming velocity ν, the equation 2.1 in frequency domain can be replaced by

$$\begin{aligned} U_o(\xi_o, \omega) &= \frac{1}{\sqrt{2\pi}} \int_{Z_i} W(\xi_i; \xi_o) \left(\frac{\sqrt{i\omega}}{4\pi D} e^{-i\omega 2D/v}\right) e^{\pm i\omega 2d(\xi_i;\xi_o)/\nu} d\xi_i, \\ &= \frac{1}{\sqrt{2\pi}} \int_{Z_i} \left(W(\xi_i; \xi_o) \frac{\sqrt{i\omega}}{4\pi D}\right) e^{-i\omega\phi(\xi_i;\xi_o)} d\xi_i, \end{aligned} \tag{2.23}$$

where $\phi(\xi_i; \xi_o) = 2D/v \pm 2d(\xi_i; \xi_o)/\nu$. For this simple case, it is easy to note that the phase $\phi(\xi_i; \xi_o)$ is stationary when $\xi_i = \xi_o$. The redatumed sample $U_o(\xi_o, \omega)$ can then be approximated by

$$\begin{aligned} U_o(\xi_o, \omega) &\approx \sqrt{\frac{1}{i\omega\phi''(\xi_o; \xi_o)}} \left(W(\xi_o; \xi_o) \frac{\sqrt{i\omega}}{4\pi D}\right) e^{-i\omega\phi(\xi_o;\xi_o)}, \\ &= \sqrt{\frac{\nu z}{2i\omega}} \left(W(\xi_o; \xi_o) \frac{\sqrt{i\omega}}{4\pi D}\right) e^{-i\omega 2(D/v\pm z/\nu)}, \\ &= W(\xi_o; \xi_o) \left(\frac{\sqrt{\nu z}}{4\pi D\sqrt{2}}\right) e^{-i\omega 2(D/v\pm z/\nu)}. \end{aligned} \tag{2.24}$$

In the case of preserving amplitudes we use $W = W_{pa}$ (equation 2.19), then we have that:

$$U_o(\xi_o, \omega) \approx W_{pa}(\xi_o; \xi_o) \frac{\sqrt{\nu z}}{4\pi D\sqrt{2}} e^{-i\omega 2(D/v\pm z/\nu)},$$

$$= \left(\frac{\sqrt{2}}{\sqrt{\nu z}}\right)\frac{\sqrt{\nu z}}{4\pi D\sqrt{2}}e^{-i\omega 2(D/v\pm z/\nu)},$$

$$= \frac{1}{4\pi D}e^{-i\omega 2(D/v\pm z/\nu)}.$$

As expected, the redatumed signal has the same amplitude as the input data (equation 2.22), thus not depending on the chosen redatuming velocity ν, and its phase is shifted by z/ν.

In the case of taking into account the geometrical spreading factor we use $W = W_{ta}$ into the Fourier inverse of equation 2.24;

$$
\begin{aligned}
U_o(\xi_o, t_o) &\approx W_{ta}(\xi_o; \xi_o)\frac{\sqrt{\nu z}}{4\pi D\sqrt{2}}\delta\left(t_o - 2(D/v \pm z/\nu)\right), \\
&= \left[\left(1 \pm \frac{2z}{\nu t_o}\right)\frac{\sqrt{2}}{\sqrt{\nu z}}\right]\frac{\sqrt{\nu z}}{4\pi D\sqrt{2}}\delta\left(t_o - 2(D/v \pm z/\nu)\right), \\
&= \left(1 \pm \frac{2z}{\nu t_o}\right)\frac{1}{4\pi D}\delta\left(t_o - 2(D/v \pm z/\nu)\right).
\end{aligned}
\tag{2.25}
$$

Note that in order to keep consistency, the $\pm$ operator chosen according to the redatuming direction, has opposite meanings on the last equation. For example, when redatuming upwards, the first occurrence is $-$ and the other is $+$. Namely, at the redatumed reflector we have

$$
\begin{aligned}
U_o(\xi_o, t_o = 2(D/v \pm z/\nu)) &\approx \left(1 - \frac{z}{D\nu/v + z}\right)\frac{1}{4\pi D}, \\
&= \left(\frac{\nu}{v}\right)\frac{1}{4\pi(D\nu/v + z)}, \\
&= \frac{1}{4\pi(D + zv/\nu)}.
\end{aligned}
\tag{2.26}
$$

The true-amplitude redatuming operator, in order to properly account for geometrical spreading, relies on a proper choose of the redatuming velocity ν. The redatumed amplitude is strongly dependent on the relation between the chosen redatuming velocity ν and the media velocity v.

2.4 Quality Factor Estimation Using Redatuming

In reflection seismology, the anelastic attenuation factor, often expressed as seismic quality factor or Q (which is inversely proportional to attenuation factor), quantifies the effects of anelastic attenuation on the seismic wavelet caused by fluid movement and grain boundary friction. As a seismic wave propagates through a medium, the elastic energy associated with the wave is gradually absorbed by the medium (Figure 2.3), eventually

ending up as heat energy. This is known as absorption (or anelastic attenuation) and will eventually cause the total disappearance of the seismic wave. Q is defined as

$$Q = 2\pi \left(\frac{E}{\delta E} \right), \tag{2.27}$$

where $\frac{E}{\delta E}$ is the fraction of energy lost per cycle (SHERIFF; GELDART, 1995). Its behaviour said to be dispersive because the rate of attenuation increases with frequency. The earth preferentially attenuates higher frequencies, resulting in the loss of signal resolution (DASGUPTA; CLARK, 1998). we describe the adopted method to estimate the Q-factor based on FPS method (ZHANG; ULRYCH, 2002) and redatuming operator (SCHNEIDER, 1978; PILA et al., 2014; OLIVEIRA; FIGUEIREDO; FREITAS, 2015).

2.4.1   One layer medium

Considering that absorption is the relation between Q-factor and the offset frequency peak (Figure 2.4), we have:
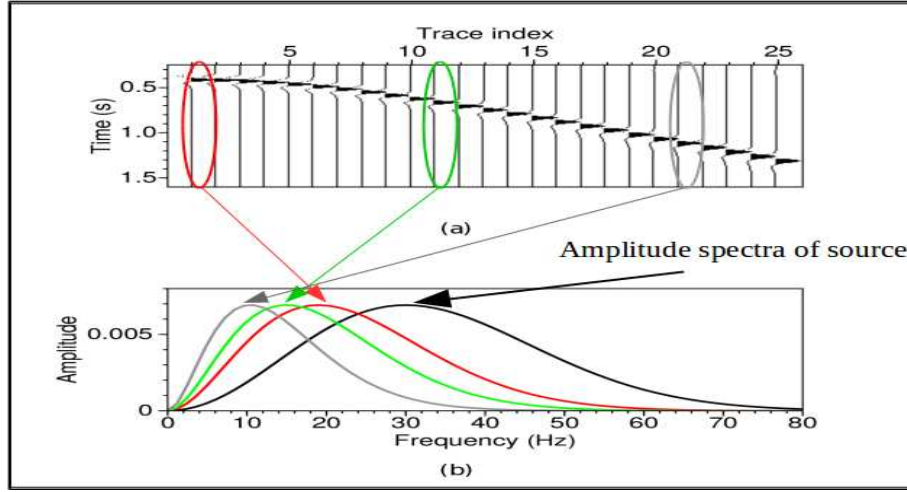
$$C(f,t) = B(f)e^{-\frac{\pi f t}{Q}}, \tag{2.28}$$

where f is the frequency, t is the time, Q the quality factor, B the amplitude of the signal and C the amplitude of attenued signal. The wave propagating absorption increases with time and, in terms of frequency distribution, the result is the translation of the high frequency bands towards lower bands.

Figure 2.3 – Seismic wave behavior in absorptive media defined by v, ρ and Q. (a) Without absorption. (b) With absorption.
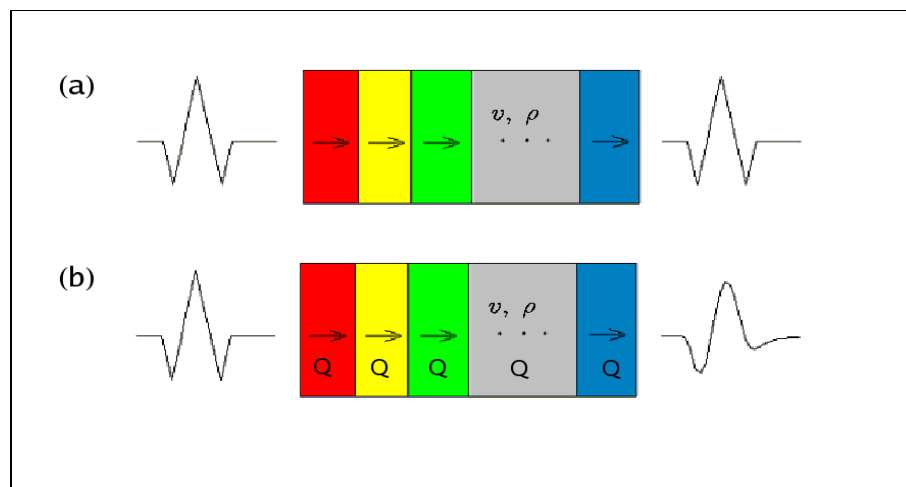
Source: From Zhang (2008)

Figure 2.4 – Seismic wave behavior in absorptive media defined by v, ρ and Q. (a) Without absorption. (b) With absorption.

Source: From author

Considering the propagation of a wave in a half-space with a Q-factor during t seconds, the amplitude spectrum of the received signal is defined by:

$$C(f,t) = A(t)B(f)e^{-\frac{\pi ft}{Q}}, \tag{2.29}$$

where $A(t)$ is an amplitude factor independent of frequency and absorption, f is the frequency, t is the time and Q is the quality factor. It is worth to mention the parameter $A(t)$ is related to other mechanisms that affect the seismic amplitude (geometrical spreading, diffractions, multiples, peg-legs, etc). Considering that the amplitude spectrum of a source can be represented by a Ricker wavelet (RICKER, 1953), the frequency spectrum is then expressed by the equation:

$$B(f) = \frac{2}{\pi} \frac{f^2}{f_m^2} e^{-\frac{f^2}{f_m^2}}, \tag{2.30}$$

where f_m is the dominant frequency. The peak frequency f_p is calculated from derivative of equation 2.29 related to frequency and equating it to zero Zhang and Ulrych (2002), and the result is:

$$f_p = f_m^2 \left[\sqrt{\left(\frac{\pi t}{4Q}\right)^2 + \left(\frac{1}{f_m}\right)^2} - \frac{\pi t}{4Q} \right]. \tag{2.31}$$

Thus, after some algebric manipulation of equation 2.31, the relationship between the quality factor and the peak frequency is defined by:

$$Q = \frac{\pi t f_p f_m^2}{2\left(f_m^2 - f_p^2\right)}. \tag{2.32}$$

Figure 2.5 – schematic representation of calculus of Q.
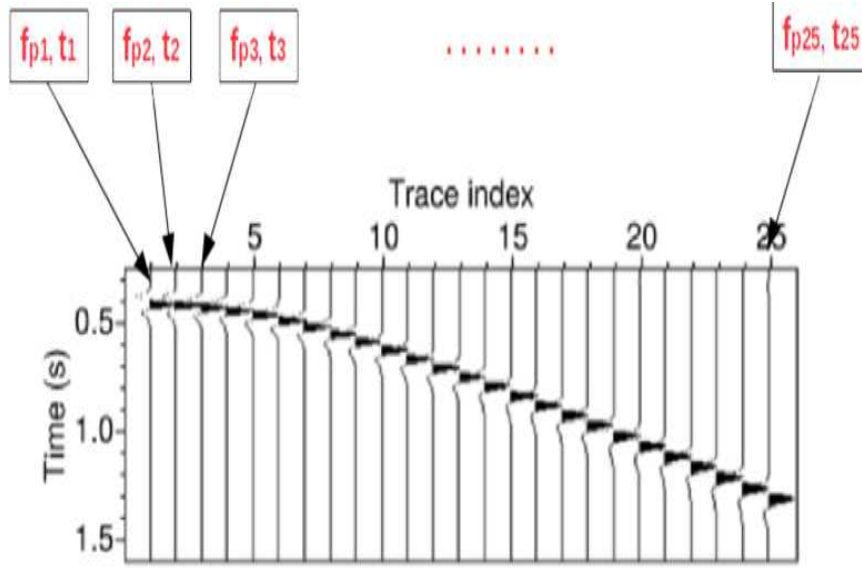
Source: From author

Considering the peak frequencies f_{p1} and f_{p2} at times t_1 and t_2 of the two consecutive seismic traces in CMP gather, the relationship between the quality factor and the peak frequency is defined by Zhang as:

$$Q = \frac{\pi t_1 f_{p1} f_m^2}{2\left(f_m^2 - f_{p1}^2\right)} = \frac{\pi t_2 f_{p2} f_m^2}{2\left(f_m^2 - f_{p2}^2\right)}. \tag{2.33}$$

It is then possible to obtain a relation between the dominant frequency and the frequency peak based on the frequency peaks of a reflection of two different traces or offsets:

$$f_m = \sqrt{\frac{f_{p1} f_{p2}\left(t_2 f_{p1} - t_1 f_{p2}\right)}{t_2 f_{p2} - t_1 f_{p1}}}. \tag{2.34}$$

The Q_m, is the average of all Q factors calculated in the offset (Equation 2.32 and is represented schematically in Figure 2.5.

2.4.2 Multi layer medium

Considering the case of a medium with two horizontal plane layers with quality factors Q_1 and Q_2 and travel times of t_1 and t_2 in each layer, respectively, Zhang and Ulrych (2002), using equation 2.29, obtained the equation:

$$C(f,t) = A(t)B(f)e^{-\frac{\pi f t_1}{Q_1}}e^{-\frac{\pi f t_2}{Q_2}}, \tag{2.35}$$

where $t = t_1 + t_2$. Later, they substituted equation 2.29 on the left side of the previous equation and replaced Q by equation 2.32. Thus Q_2 can be defined by:

$$Q_2 = \frac{\pi t_2 Q_1}{\alpha Q_1 - \pi t_1},$$
(2.36)

where

$$\alpha = \frac{2f_m^2 - 2f_p^2}{f_p f_m^2}.$$
(2.37)

For a multi-layers medium with horizontal plain, equation 2.29 reads:

$$C(f,t) = A(t)B(f)e^{\left(\sum_{i=1}^{N} \frac{\pi f \Delta t_i}{Q_i}\right)},$$
(2.38)

where Q_i and Δt_i are the quality factors and the travel time in layer i, respectively. In accordance to the simplification of the ray propagation, the travel time of a particular offset was defined by:

$$\sum_{i=1}^{N} \Delta t_i = t_N,$$
(2.39)

and

$$\Delta t_i = \frac{t_N}{t_o(N)} \left[t_o(i) - t_o(i-1) \right],$$
(2.40)

where Δt_i is the travel time in each layer determined by triangularization, t_N is the total time of reflection of a particular offset and $t_o(N)$ is the vertical time reflection in layer N.

Considering a medium with N horizontal layers with quality factors $Q_1, Q_2, ..., Q_N$, respectively, an equation was analytically defined in order to calculate each quality factor:

$$Q_N = \frac{\pi \Delta t_N}{\alpha - \beta},$$
(2.41)

where α was previously defined and β is defined by:

$$\beta = \sum_{i=1}^{N-1} \frac{\pi \Delta t_i}{Q_i}.$$
(2.42)

2.4.3 Analysis of methodology

The method of Zhang shows a limitation due the trajectory of the wave field as a straight ray. We can observe that there is a difference between the propagation time using Snell's law and considering a straight ray (see Figure 2.6). This error will certainly grow with increasing of distance. Thus, we notice that the estimation of Q factors dependent of a good estimate of the wavefield propagation time in each layer, and the approximation by equation (2.40) does not allow a good approximation.

The redatuming operator is used to repositioning the wavefield of acquisition system, simulating the acquisition at another level and iteratively correcting the travel time

(BERRYHILL, 1984; PILA et al., 2014; OLIVEIRA; FIGUEIREDO; FREITAS, 2015). In previous works (PILA et al., 2014; OLIVEIRA; FIGUEIREDO; FREITAS, 2015), the true-amplitude redatuming operator has been developed to recover the amplitude related to the geometrical spreading in the zero-offset domain. This means, it was performed a dynamic correction of signal. In this work, we used this operator only in the kinematic context, considering the weight function equal to one, thus providing only the correction of traveltime. For this purpose, the redatuming operator does not show any limitation related to the type of offset.

The redatuming operator in the frequency domain does not consider the geometrical spreading correction, only the travel time (SCHNEIDER, 1978), and is defined by:

$$P(r_s, \omega) = \int_x \frac{\partial r}{\partial n} \sqrt{i\omega} P(r, \omega) \frac{e^{i\omega t}}{\sqrt{r}} dx, \quad (2.43)$$

where $P(r, \omega)$ is the input field and $P(r_s, \omega)$ is the simulated field in the new level, ω is the frequency and r the distance between the original position acquisition and the output position at the new level. Thus, performing the redatuming operator, we can strip the layers one by one, and then use the redatumed time in the new layer associated with equation 2.32.

Figure 2.6 – Schematic of the straight ray and of the Snell ray.
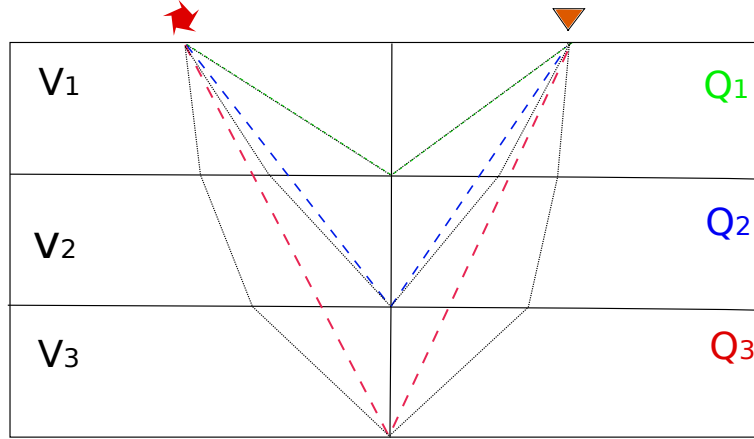
Source: From author

In a schematic representation for a model with three horizontal plane layers (Figure 2.7), the travel time of each offset for the first layer are identical, allowing to have an approximation near of the exact value of Q in the first layer.

For the second layer, the relationship would be:

$$\Delta t_2' = \frac{t_2}{t_o(2)} (t_o(2) - t_o(1)), \quad (2.44)$$

and

$$\Delta t_1' = t_2 - \Delta t_2', \tag{2.45}$$

that are results of the travel times of the rays in blue for the second layer. For the third layer, the travel times of the segments of the red ray will be determined by

$$\Delta t_3^* = \frac{t_3}{t_o(3)} \left(t_o(3) - t_o(2)\right), \tag{2.46}$$

where

$$\Delta t_2^* = \frac{t_3}{t_o(3)} \left(t_o(3) - t_o(1)\right) - \Delta t_3^*, \tag{2.47}$$

and

$$\Delta t_1^* = t_3 - \Delta t_2^* - \Delta t_3^*. \tag{2.48}$$

Generalizing, we can conclude that the equations for determining the travel times of the segments of the rays in each layer are defined by

$$\Delta t_N^* = \frac{t_N}{t_o(N)} \left(t_o(N) - t_o(N-1)\right),$$

$$\Delta t_{N-1}^* = \frac{t_N}{t_o(N)} \left(t_o(N) - t_o(N-2)\right) - \Delta t_N^*,$$

$$\vdots$$

$$\Delta t_1^* = t_N - \ldots\ldots - \Delta t_{N-1}^* - \Delta t_N^*. \tag{2.49}$$

Figure 2.7 – Schematic propagation of the straight ray and the traveltime in each layer.
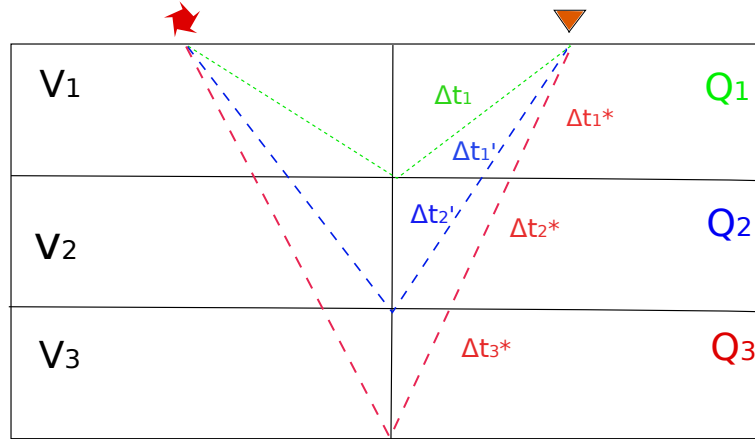
Source: From author

Despite the correction in the equations of the transit times in the layers have been applied, the estimated results of the quality factors did not approach the exact values. For this reason we use the redatuming operator to correct the transit times using the RMS (root means square) velocities and interval velocities according to the following equations:

$$V_{RMS}^2 = \frac{\sum\limits_{i=1}^{N} V_i^2 \Delta t_i}{\sum\limits_{i=1}^{N} \Delta t_i}, \tag{2.50}$$

with V_{RMS} the RMS velocity, V_i the interval velocity and Δt_i is the double time interval considering zero offset for the i th layer, and N is the number of layers and the interval velocity given by

$$V_N^2 = \frac{V_{RMSN}^2 T(0)_N - V_{RMSN-1}^2 T(0)_{N-1}}{T(0)_N - T(0)_{N-1}},$$ (2.51)

where V_N is the interval velocitie, V_{RMSN} and V_{RMSN-1} are the RMS speeds of the top and bottom layers to the nth layers, and $T(0)_N$ and $T(0)_{N-1}$ their trajectory from time considering offset zero.

Below in Figure 2.8 we can see the processing flow conducting the redatuming, measurement of Q factor and application filtering Q.

Figure 2.8 – Workflow of seismic processing.
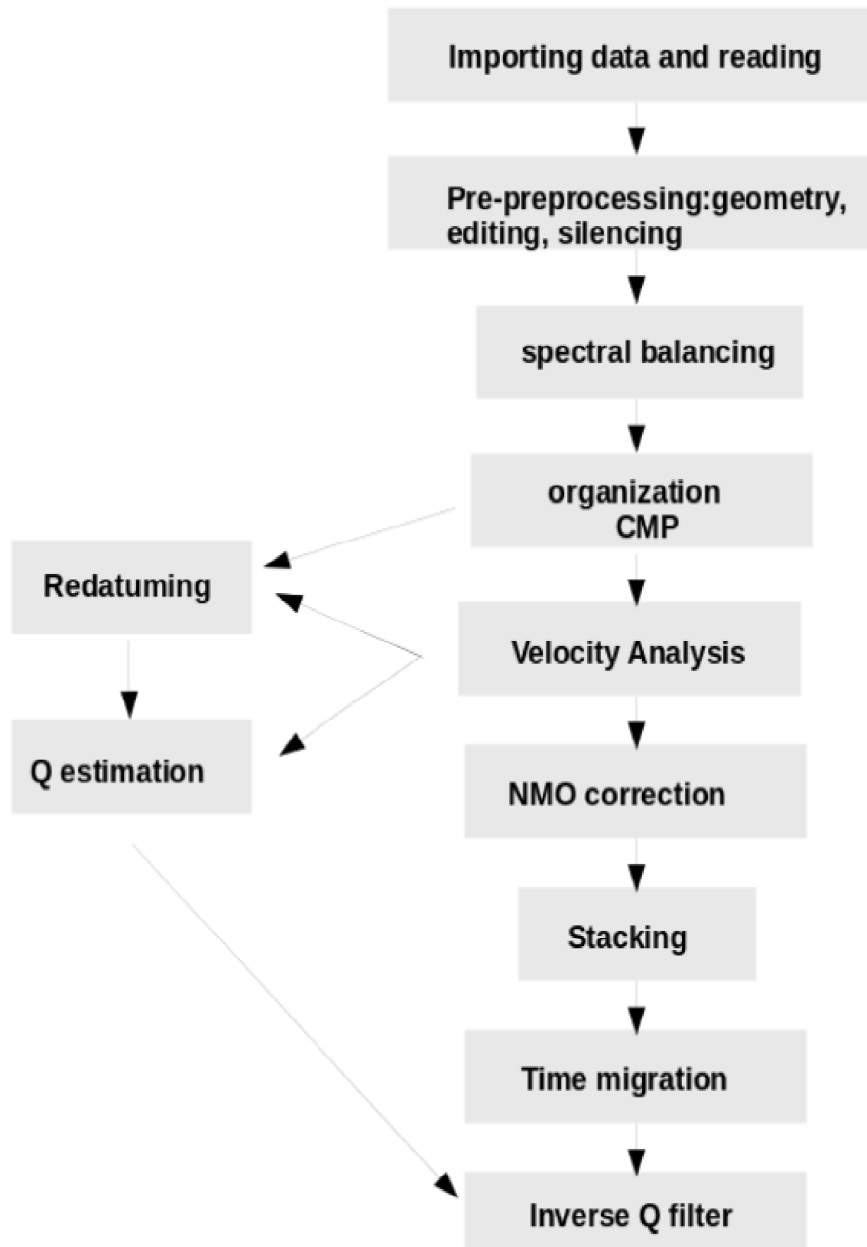
Source: From author

3 RESULTS

In this chapter we show the results of the redatuming operator analysis as well as the estimative of quality factor obtained by the redatuming operator and frequency shift method.
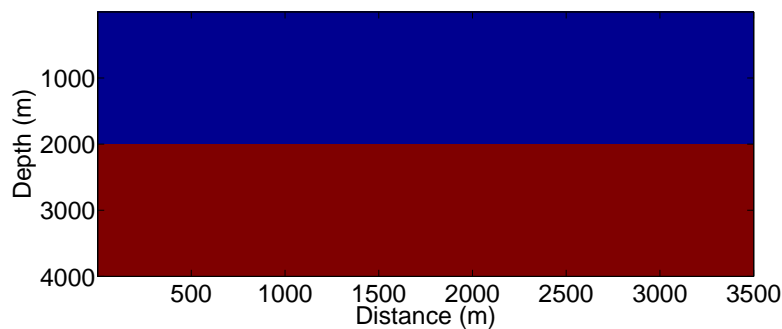
3.1 Redatuming in True Amplitude

About the redatuming operator, the results of the analysis of amplitude and travel time with a variation in the velocity model was shown by numerical and real data sets. We analysed three numerical examples, and on a real GPR data set. The GPR data were used because the half-offset are short and the configuration of this data is similar to a zero-offset.

3.1.1 Model I: two horizontal layers

In this synthetic example, we apply redatuming operators in a horizontally layered model with two horizontal homogeneous layers, where the first acoustic wave velocity background is $v_1 = 1500$ m/s and the second $v_2 = 2200$ m/s, and is depicted in Figure 3.1. The zero-offset dataset (Figure 3.2a) was simulated with a 25 Hz Ricker wavelet by Kirchhoff modeled and sampled on the time at 4 ms spaced in every 10 m. Its measurement level is constant at level $z = 0$ m. Another dataset used as reference was simulated with the measurement level equal to the target output datum ($z = 1000$ m) with identical parameters (see Figure 3.2b). his datum in new level is located to 50% of the depth in first layer.

Figure 3.1 – Velocity model of two homogeneous layers (Model I), where the first layer velocity is 1500 m/s and the second 2200 m/s.
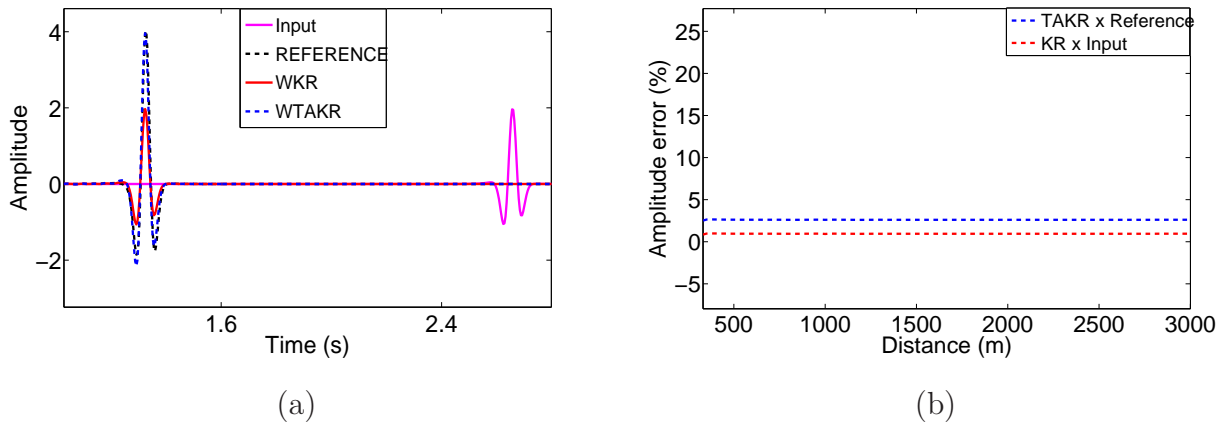

Source: From author

The output of both true-amplitude and conventional redatuming operators are presented in Figures 3.2c and 3.2d. A single-trace detailed comparison is presented in Figure 3.3a. As expected, both operators give results of traces kinematically equal to the reference trace. On the other hand, while the output from the conventional operator has the same amplitude as the input, the true-amplitude operator yields traces with the same amplitude as the reference trace. As can be noted on Figure 3.3b, the amplitude erros are low.

Figure 3.2 – Model I datasets: (a) input, (b) reference data, (c) amplitude-preserving redatuming result, and (d) true-amplitude redatuming result.
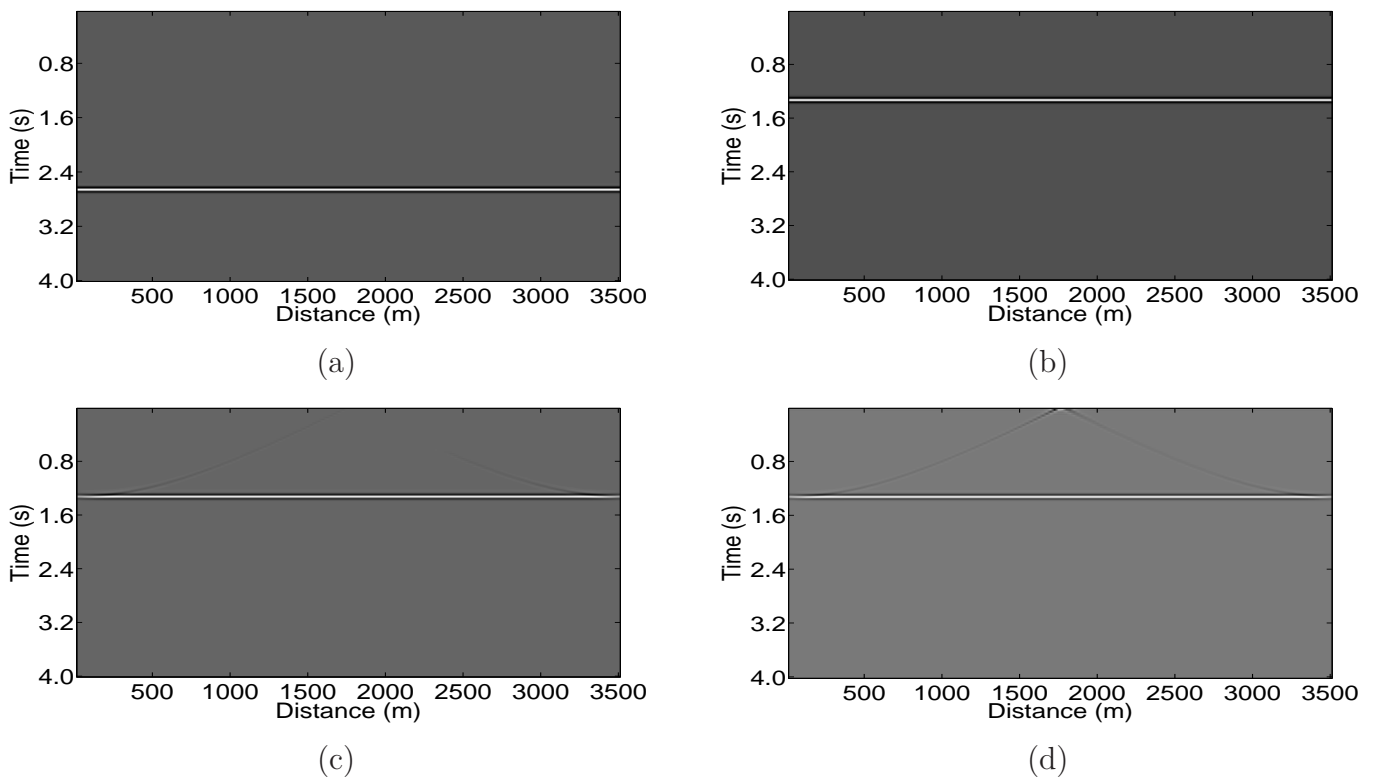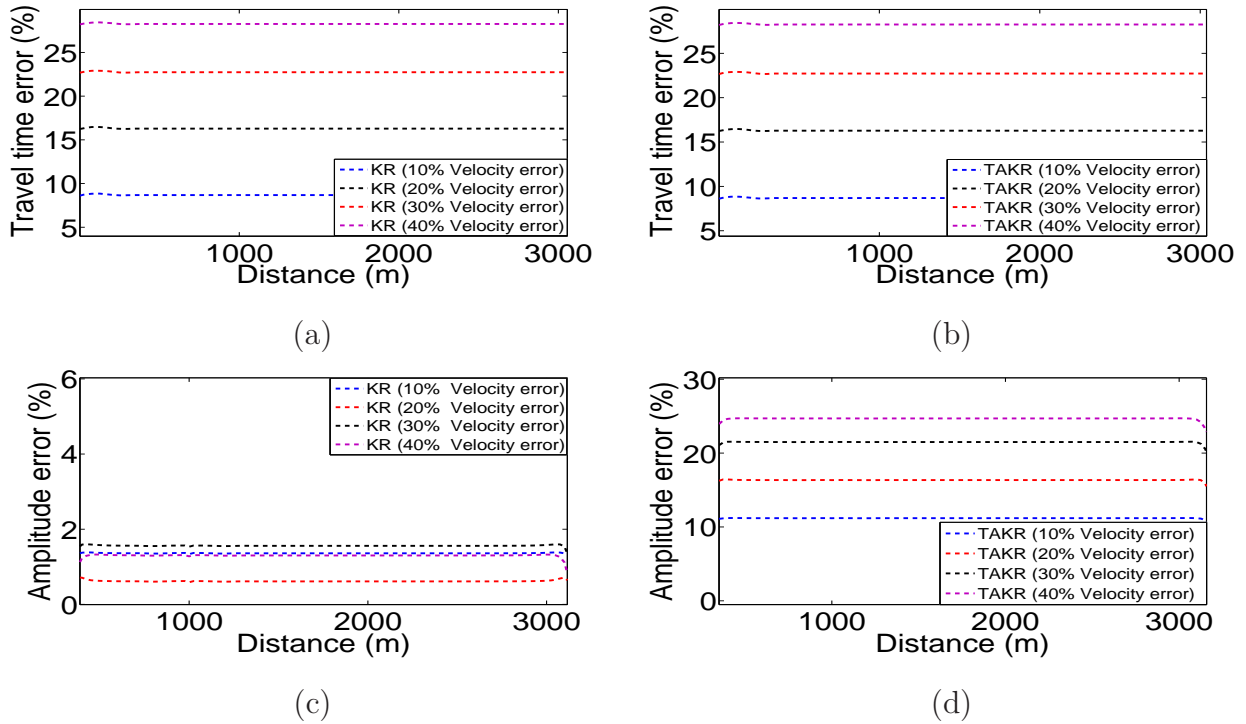

Source: From author

Figure 3.3 – (a) Input seismic trace (purple), reference (black dashed), KR (red) and TAKR (blue dashed). The KR and TAKR results were repositioned with the weight function (2.15) and (2.20) respectively and the redatuming in this case recovered the correct amplitude. (b) The relative amplitude errors between the TAKR data and the reference (blue line) are around 3.5 %. The relative error between the KR and the reference data (red line) is around 1%.

(a)   (b)

Source: From author

A second experiment on the same model aimed at to analyse the velocity sensitivity of the Kirchhoff redatuming (KR) and true amplitude Kirchhoff redatuming (TAKR) operators. Since the operators are kinematically the same, the error in travel-time are identical (see Figure 3.4a and 3.4b). On the other hand, as commented in Subsection 2.3.1, while the amplitude of the conventional operator is independent of the velocity error, the true-amplitude operator is sensitive to it. The errors of the amplitude-preserving operator remain 7%, even for velocity errors of 40%, while the true-amplitude operator errors reach 27% in this model.

Figure 3.4 – Velocity error plots and traveltime error for (a) amplitude-preserving and (b) true-amplitude redatuming operators and the respective amplitude errors shown in (c) and (d).
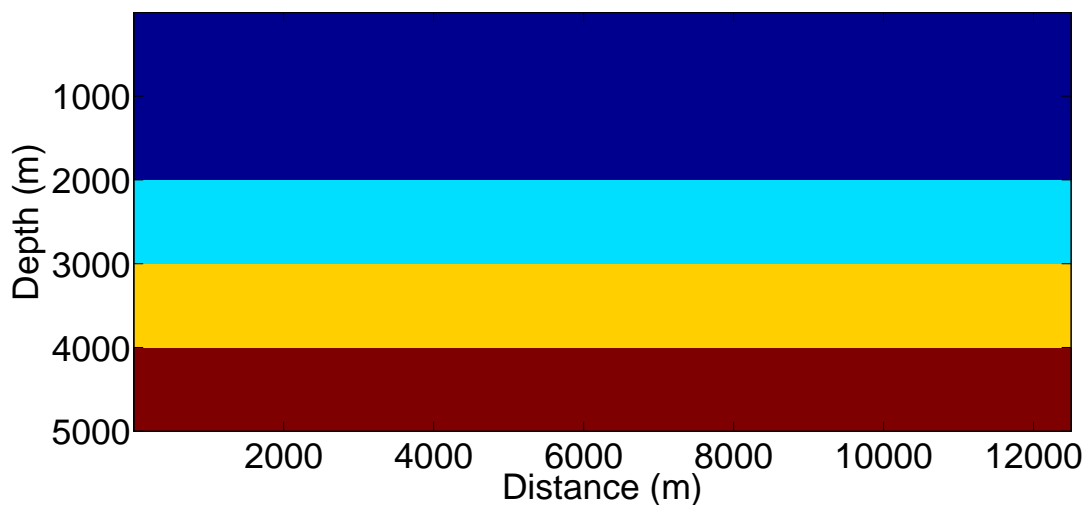

Source: From author

As it can be seen, both operators present accurate results, either preserving or adjusting the amplitude. However, in order to obtain an estimate of the geometrical spreading, the true-amplitude operator relies on a proper velocity model. The analytic analyses and numerical experiments show that the amplitude error for this operator is strongly affected by errors in the velocity field.

3.1.2 Model II: four horizontal layers

Here, in order to verify the feasibility of both operators when V_{RMS} velocities are taken into account, we generated a second model which consists of four horizontal homogeneous layers as depicted in Figure 3.5. The depth interval velocities of this model were 1500 m/s, 2000 m/s, 2500 m/s and 3000 m/s.

Figure 3.5 – Velocity model with four homogeneous layers with velocities 1500 m/s, 2000 m/s, 2500 m/s and 3000 m/s (Model II).
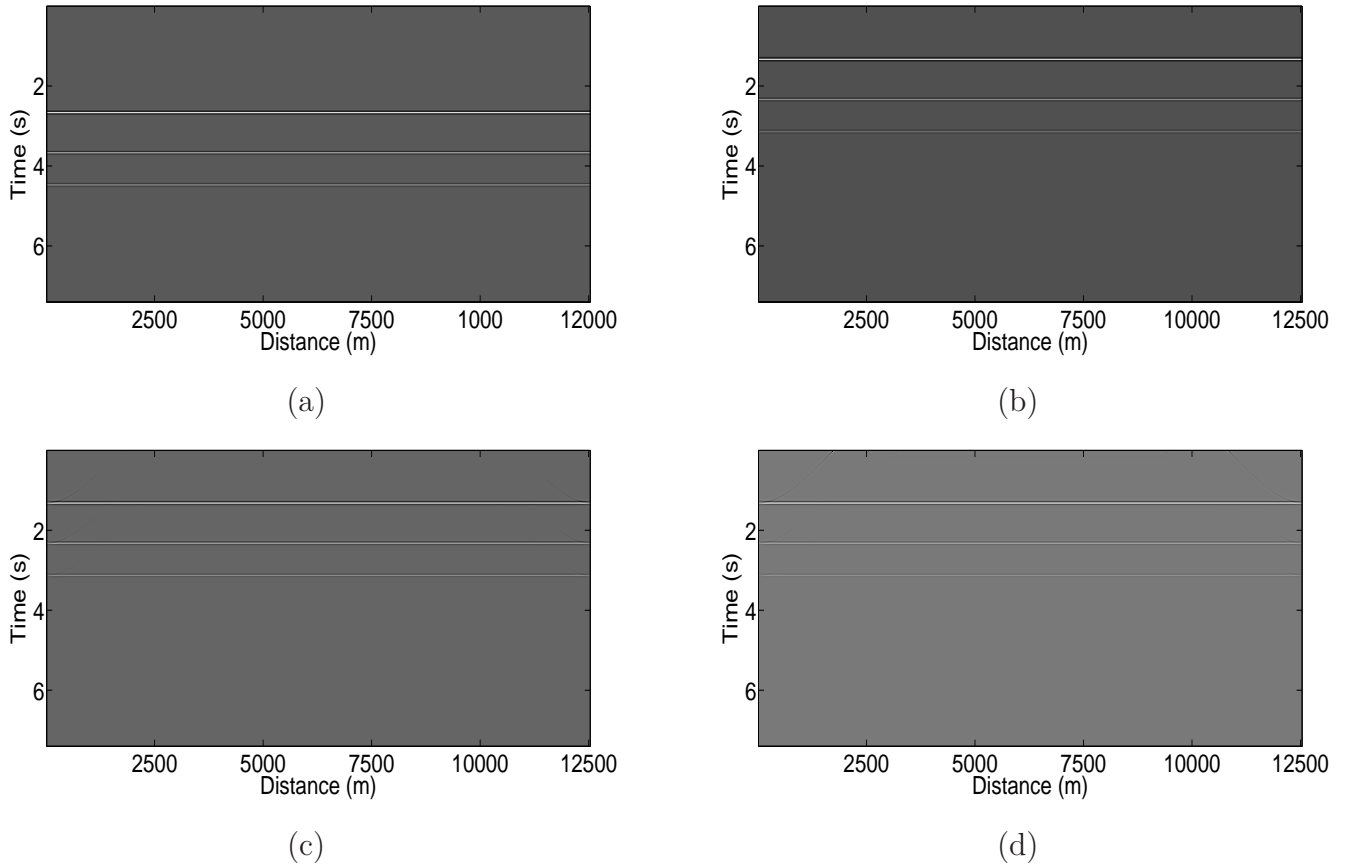

Source: From author

The source-receiver pairs were positioned at every 25 m. The data was modelled by Trisies (from Seismic Unix) which uses a Gaussian beam operator to produce true-amplitude synthetic seismograms with a Ricker wavelet of 25 Hz. This seismogram was used as an input for KR operator in zero-offset. The zero-offset dataset, shown in Figure 3.6a has a sampling ratio of 4 ms, and the measurement level is constant at $z = 0$m. Another dataset, to be used as reference, was simulated having the measurement level equal to the target output datum ($z = 1000$m) with identical parameters (see Figure 3.6b) also calculated by Trisies.

The outputs of both true-amplitude and conventional redatuming operators are presented in Figures 3.6c and 3.6d. One-trace detailed comparisons are presented in Figures 3.7 and 3.8. Just like the first experiment, both operators presented good accuracy in their kinematic and dynamic purposes.

Figure 3.6 – Model II datasets, (a) input, (b) reference, (c) amplitude-preserving, and (d) true-amplitude redatuming operators.

(a)

(b)

(c)

(d)

Source: From author

Figure 3.7 – Single-trace comparison of Model II datasets.
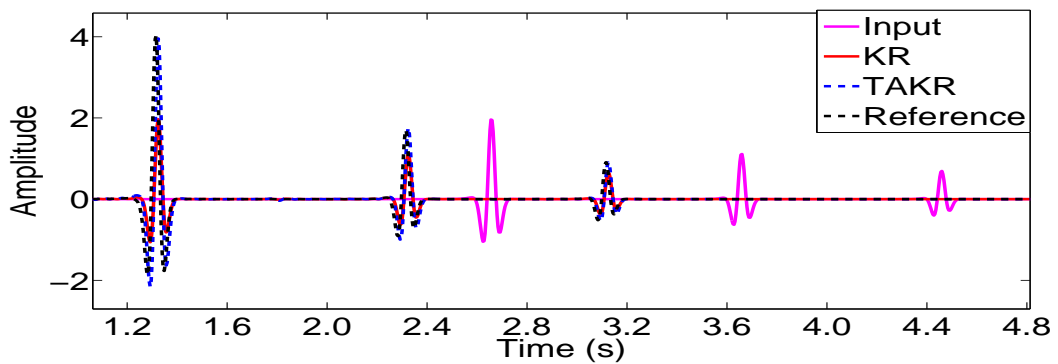
Source: From author

Figure 3.8 shows that the V_{RMS} velocity is used in the redatuming operation, the error between the KR and input data set is less than 1% for all layers, even the deepest one. However, in the case of TAKR redatuming the error is more sensitive to differences between true and V_{RMS} velocities. Based on what Subsection 2.3.1 shows, the TAKR is more sensitive to velocity error. The deeper the layer, the more V_{RMS} moves away from interval velocity. It is expected the that TAKR operator be more sensitive to velocities of the deeper layers.
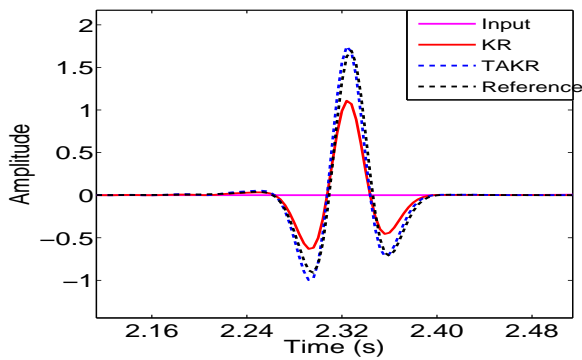
Figure 3.8 – Detailed comparison: (a), (c) and (e) one single-trace zooms for the first, second and third events; (b), (d) and (f) multi-trace amplitude error plot for first, second and third events.
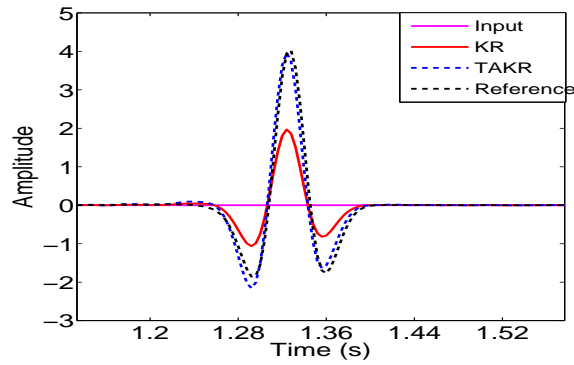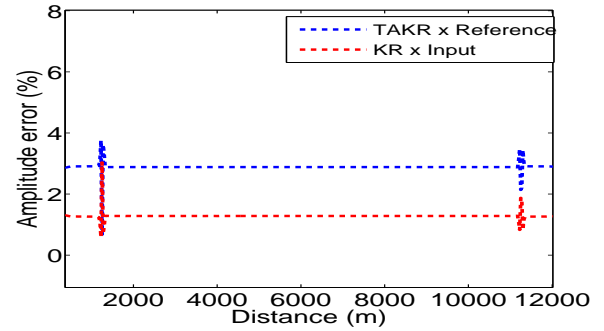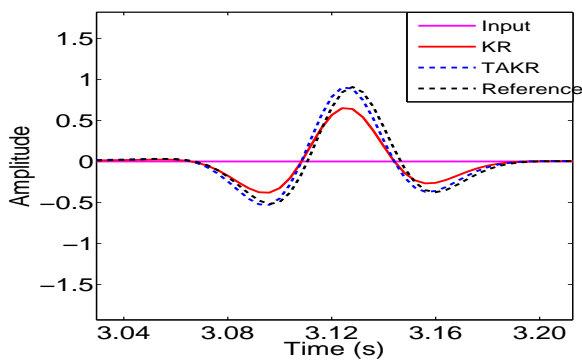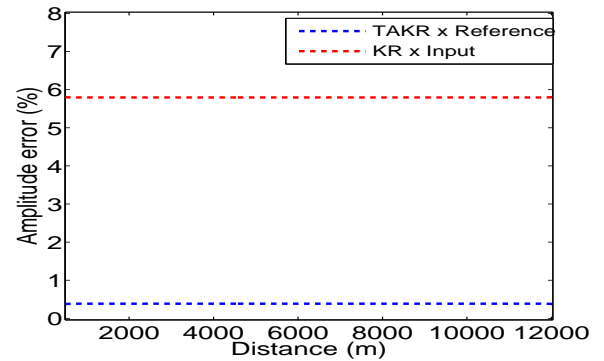

(a)
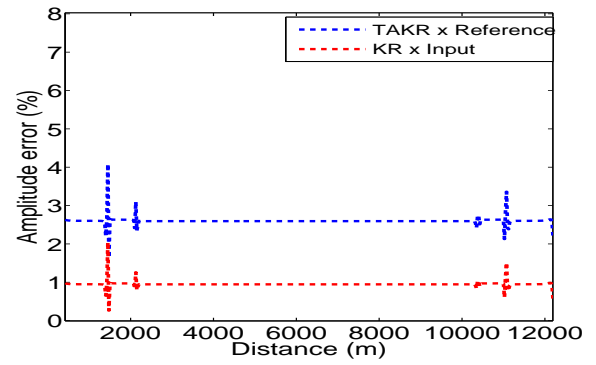
(b)

(c)

(d)

(e)

(f)

Source: From author

3.1.3   Model III: four curved layers

The third model consists of four curved homogeneous layers as depicted in Figure 3.9. The zero-offset dataset (Figure 3.10a) was simulated with a 25 Hz Ricker wavelet by Gaussian beam modelling, sampled at 4 ms and 10 m, and its measurement level is constant at $z = 0$ m. Another dataset, to be used as reference, was simulated having the measurement level equal to the target output datum ($z = 200$ m) with identical parameters (see Figure 3.10b).

Figure 3.9 – Velocity model with four curved layers with velocities 1581 m/s,1690 m/s, 1826 m/s and 2000 m/s (Model III).
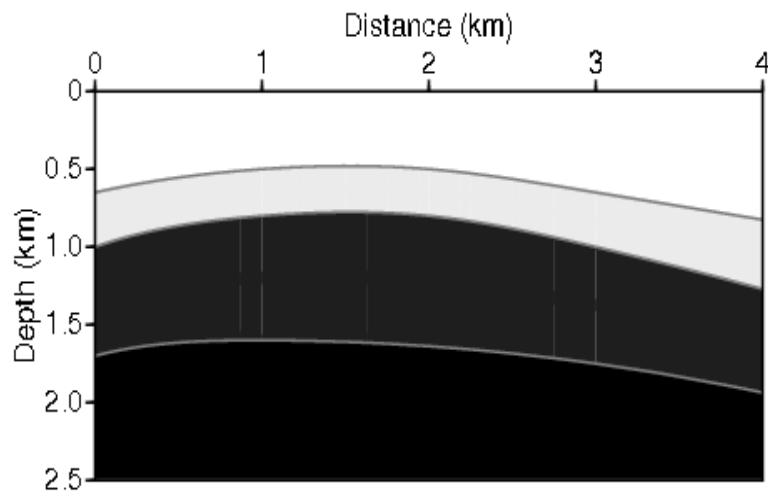
Source: From author

The output of both true-amplitude and conventional redatuming operators are presented in Figures 3.10c and 3.10d. One-trace detailed comparison is presented in Figure 3.11.

Figure 3.10 – Model III datasets: (a) input, (b) reference and outputs of (c) amplitude-preserving, and (d) true-amplitude redatuming operators.

(a)   (b)

(c)   (d)
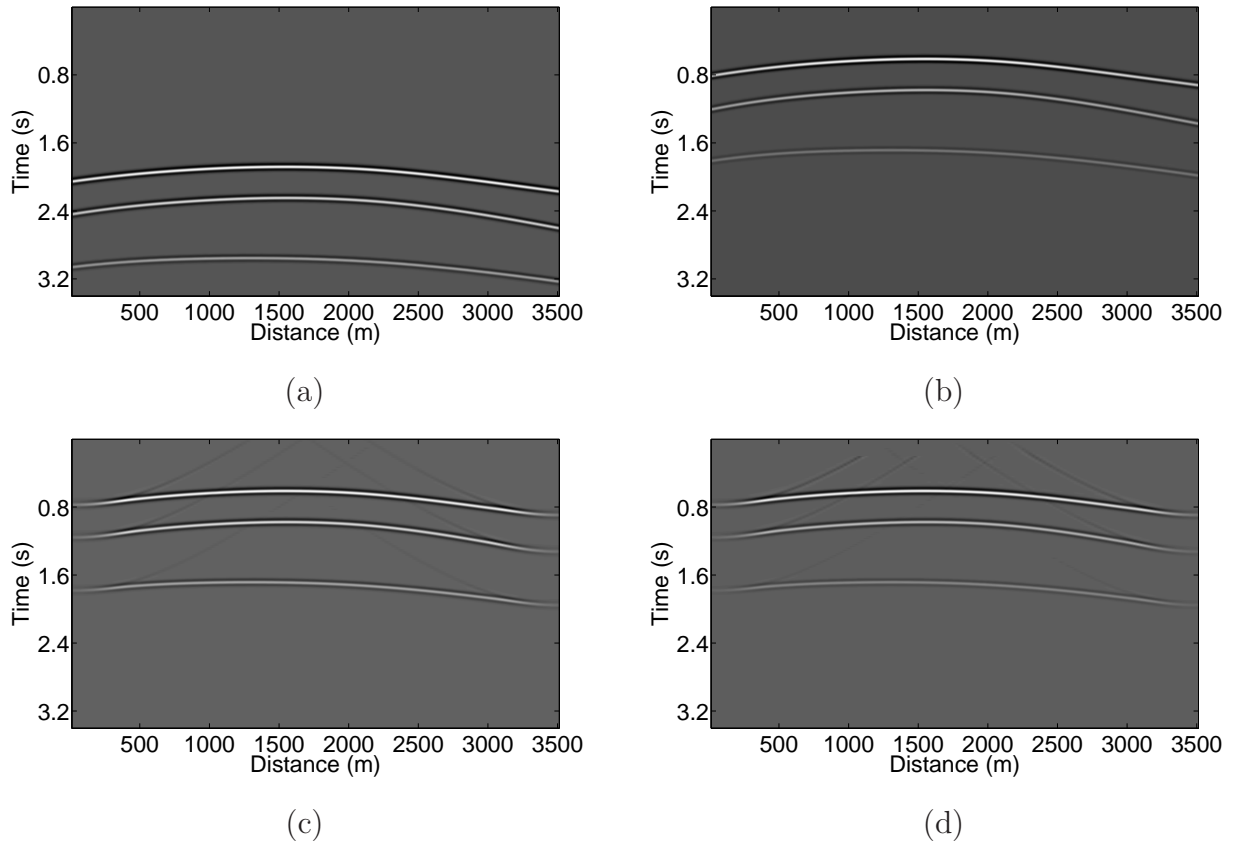
Source: From author

Figure 3.11 – Single-trace detailed comparison of Model III datasets.
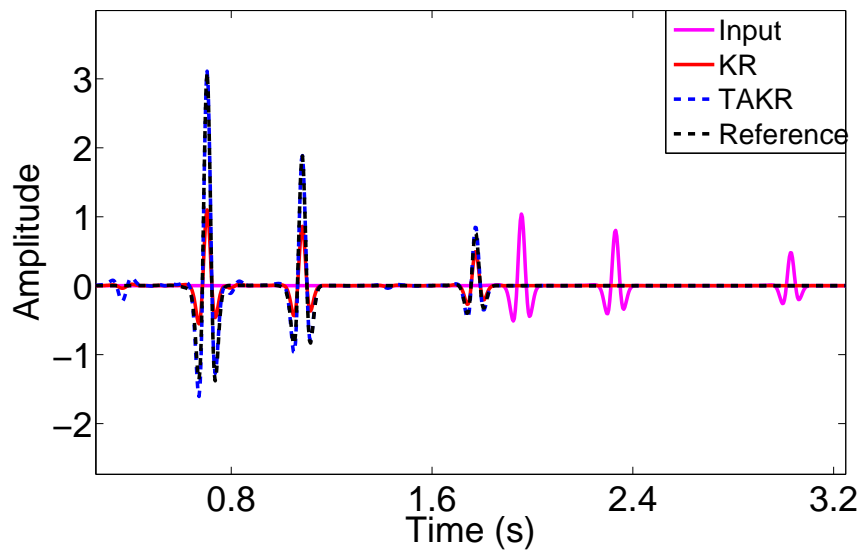
Source: From author

Figure 3.11 compares the central trace of the KR and TAKR data with the central trace of the input and the reference sections. Just like in the model with four layers, this experiment showed that the difference in amplitude between the KR response and the input data is still the same with the increase of depth, and the TAKR response and reference data increased with the increase of time. However, when it comes to amplitude recovering, the TAKR profile has the amplitude recovering factor.

3.2 Field Data Example: Ground Penetrating Radar (GPR) dataset

Siple Dome (81.65° S, 148.81° W) is an ice dome which is approximately 100 km wide by 100 km long, located 130 km east of Siple Coast in Antarctica. This dome is particularly important for determining the current mass balance of the West Antarctic ice sheet (WAIS).

The GPR survey was performed at a specific location indicated in red line in Figure 3.12a. Figure 3.12b shows a slice of the 100 MHz GPR profile acquired in Siple Dome. The distance between the transmitter and receiver antennas was $1.0\ m$ (half-offset, $h = 0.50\ m$), and the interval between traces was $0.75\ m$. A total of 8000 traces was collected along the $6000\ m$ survey line. But here, for observation issues we are showing a spatial window of 3000 m (see Figure 3.12b). The length of the time window was 913 ns and the number of samples per trace was 1870, resulting in a time sampling rate of $0.49\ ns$.

Figure 3.12 – (a) Map of location of Siple Dome in eastern Antarctica, Antarctic Explores. (b) Input GPR data 100 MHz acquired in Siple Dome.

(a)   (b)
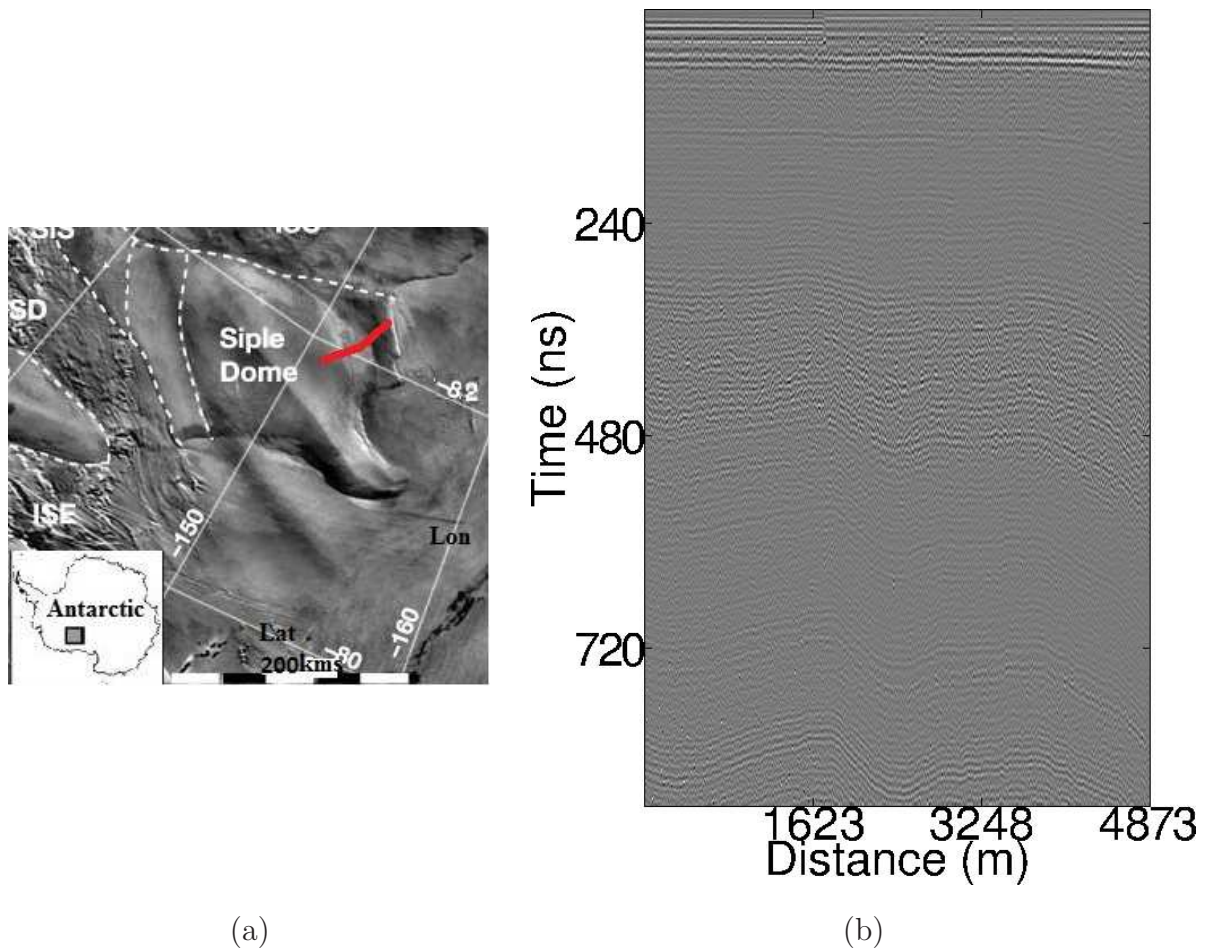
Source: (a) From Catania, Hulbe and Conway (2010) and (b) From author

As an example, we applied both operators to the profile of Figure 3.12b, redatuming it to a flat output datum located at 15m depth. On the first example we used the ice velocity (0.16 m/ns) to redatuming (ALLEY; BENTLEY., 1988). As expected, the difference between the two results is purely dynamic (see Figure 3.13). While the conventional amplitude-preserving operator maintains the relativeness of the input profile (Figure 3.13a), the true-amplitude operator increases the amplitudes on the first 300 ns of the section. This enhancement is more evident on the shallow part due to the bigger ratio between the acquired and adjusted geometrical spreading factors.

Figure 3.13 – Application of (a) amplitude-preserving, and (b) true-amplitude redatuming operator to profile of Figure 3.12b.

(a)

(b)
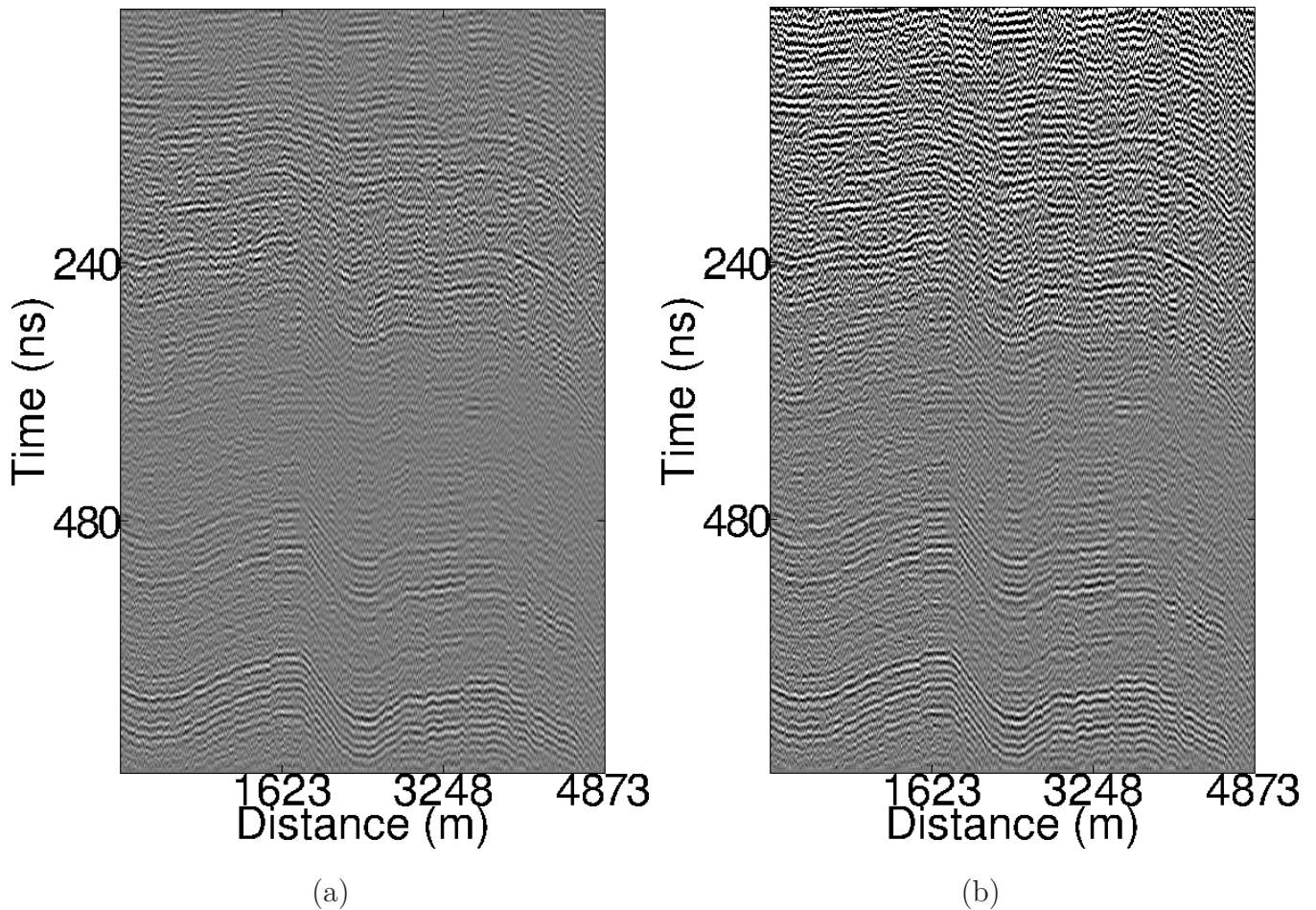
Source: From author

As a second example, we simulated a non accurate velocity field, choosing a 50% higher redatuming velocity (0.24 m/ns). As showed in the previous sections, Figure 3.14 illustrates the impact of velocity error on both redatuming operators. Note that Figures 3.13a and 3.14a present similar amplitude responses. On the other hand, the amplitude response of the true-amplitude operator is affected by the velocity error (see Figures 3.13b and 3.14b).

Figure 3.14 – Illustration of using an inaccurate velocity field for (a) amplitude-preserving, and (b) true-amplitude redatuming.

(c)

(d)
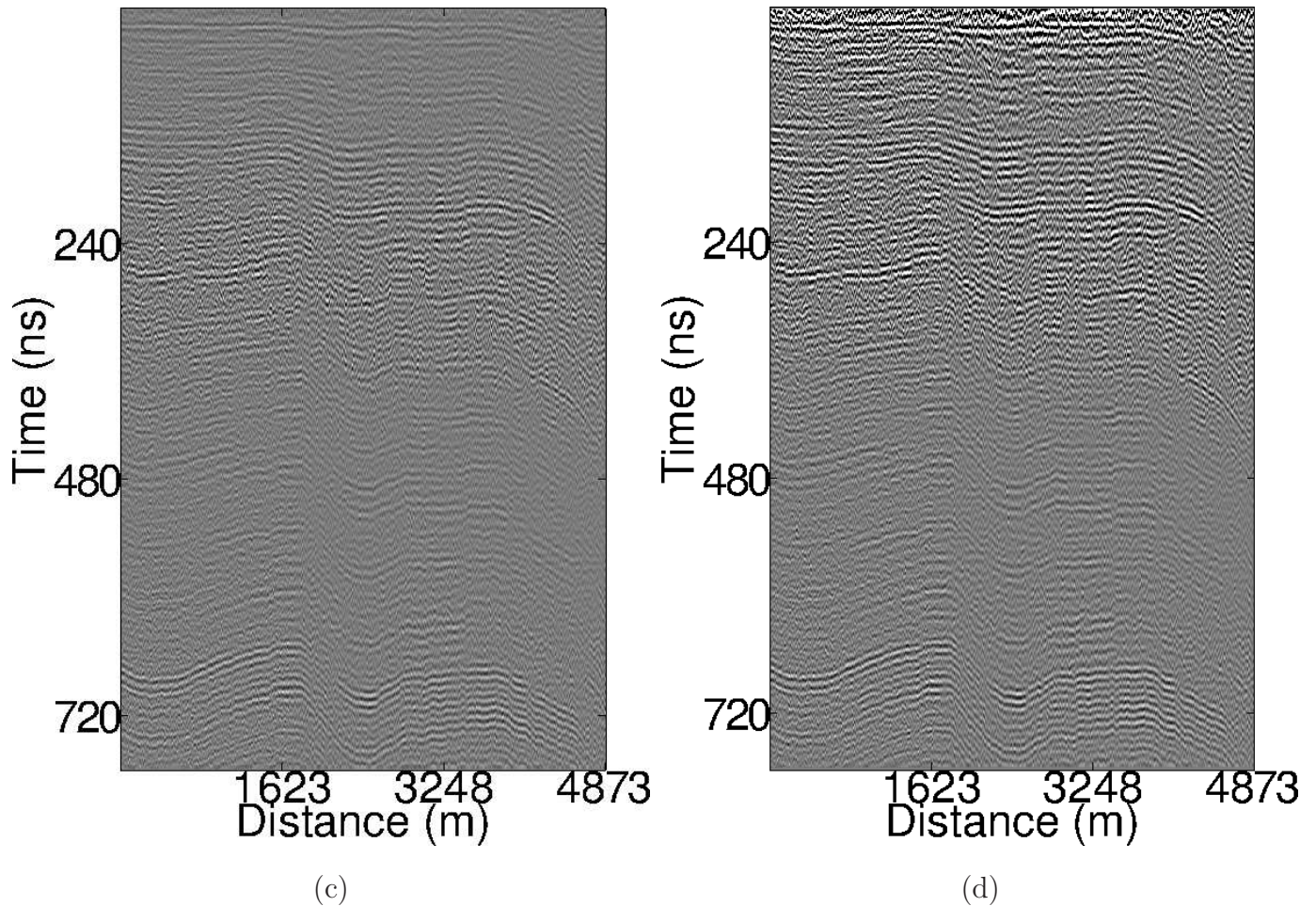
Source: From author

As it can be seen in both cases (with correct and wrong velocity) the amplitude at the deepest layers is highlighted for TAKR operation. In other words, the events presented better lateral continuity when compared with the TK result. We can observe this characteristics on the first events on the top of the data, on the left side around 300 ns and at the end in 700 ns.

3.3 Quality Factor Estimation

We applied the method to obtain the quality factors in two synthetic attenuated data, and in the real Viking Graben data set.

3.3.1 Model I: medium with horizontal plane multilayer

In this case, the model was generated using TRIMODEL from Seismic Unix and it consists of horizontal-plane layers (see Figure 3.15). The velocity model consists of 5 layers horizontal plane with velocities of $v_1 = 1508 \ m/s$, $v_2 = 2000 \ m/s$, $v_3 = 2132 \ m/s$, $v_4 = 3015 \ m/s$ and $v_5 = 3333 \ m/s$, respectively. The attenuation factor for the layers were $Q_1 = 80$, $Q_2 = 120$, $Q_3 = 160$ and $Q_4 = 200$ (Figure 3.15). The seismic data was generated by TRISEIS from Seismic Unix, which computes synthetic seismograms using Gaussian beams. The data were organized in CDP families, and the CDP chosen for analysis was the number 501 (shown in Figure 3.16). The next step was to recursively perform the redatuming in order to calculate the travel times in each layer. Then we used the attenuated modeled data and the new redatumed time together to obtain the quality factor using equation 2.32.

The results showed a good estimate of the quality factors when using the interval velocity and/or the RMS velocity in the redatuming operator, and the results given in Table 3.1. Where we observe that the errors in the estimation of the quality factors (Q_1 and Q_2) are low in "Error 1" column, but are not very different from the values in "Error 2" and "Error 3" columns. In the last two values (Q_3 and Q_4) the relative errors in "Error 1" column are much higher than the values in "Error 2" and "Error 3" columns. As, a conclusion the estimated quality factors with time correction, using redatuming, showed better results. In order to verify the robustness of our method, we perturbed the velocity models with an error of 10 %, and Table 3.2 shows the results in details. Note that even using a error in the velocity, the estimations are still good.

In both cases, with or without error in velocity model, we can notice in Figures 3.17 and 3.18 that the estimated quality factors with redatumed data for interval velocity (green point) and for RMS velocity (black point) are close to the exact value (blue point), in contrast to the results obtained by Zhang and Ulrych (2002) (in red), which showing good results only in the first two values, being different from the true value (blue point)

Figure 3.15 – Velocity model with 5 plane horizontal homogeneous layers.
in the last two estimated results.
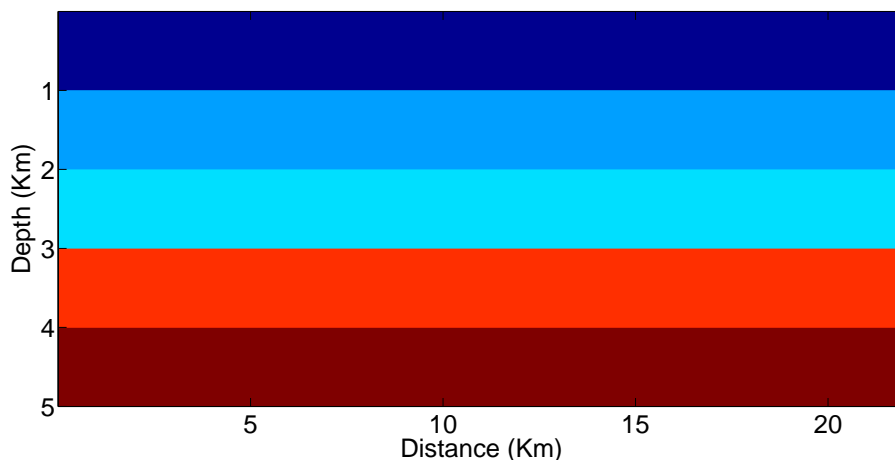
Source: From author
Figure 3.16 – Input attenuated data (CMP 501).
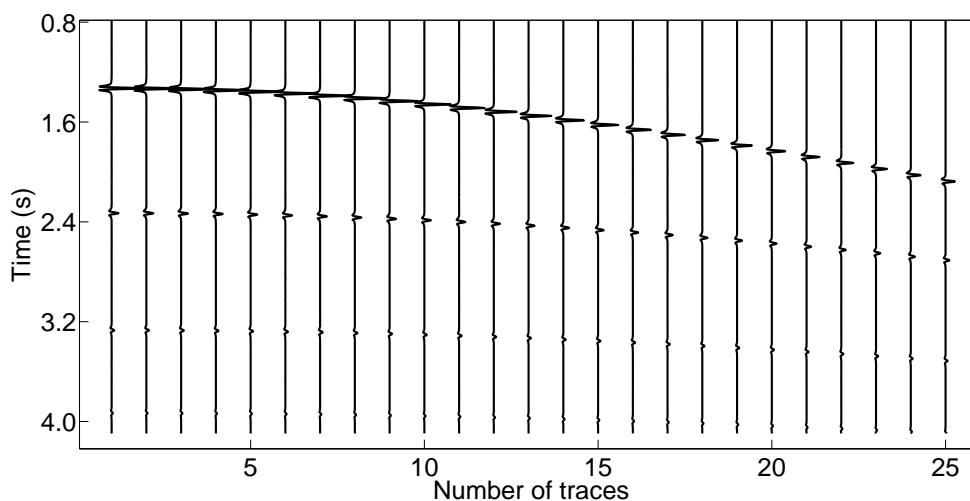
Source: From author

Table 3.1 – Quality factor estimations. In the first column the exact Q values. In the second, the
values estimated by Zhang and Ulrych (2002). The third column depicts the estima-
tive of the quality factors using interval velocity and the fourth the estimative using
RMS velocity. The others columns show the relative errors of Zhang and Ulrych
(2002), PFS with time correction of redatuming using interval velocity and PFS
with time correction of redatuming using RMS velocity, respectively

|	Exact	Zhang & Ulrych	Interval vel.	RMS vel.	Error 1	Error 2	Error 3
Q_1	80	80.64	80.64	80.64	0.8%	0.8%	0.8%
Q_2	120	121.03	125.97	125.97	0.8%	5%	5%
Q_3	160	276.35	150.90	128.38	72%	5.6%	19.75%
Q_4	200	533.66	169.03	186.45	166%	15.5%	6.7%

Source: From author

Table 3.2 – Quality factor estimated with an error of 10% in the interval velocity and RMS velocity. In the second, the values estimated by Zhang and Ulrych (2002). The third column depicts the estimative of the quality factors using interval velocity and the fourth the estimative using RMS velocity. The others columns show the relative errors of Zhang and Ulrych (2002), PFS with time correction of redatuming using interval velocity and PFS with time correction of redatuming using RMS velocity, respectively

|	Exact	Zhang & Ulrych	Interval vel.	RMS vel.	Error 1	Error 2	Error 3
Q_1	80	80.64	80.64	80.64	0.8%	0.8%	0.8%
Q_2	120	119.67	134.68	134.68	0.2%	12%	12%
Q_3	160	277.56	131.52	160.77	73%	17.8%	0.5%
Q_4	200	512.66	261.55	135.45	156%	30%	32%

Source: From author

Figure 3.17 – Q estimated with redatumed data for interval and RMS's velocities. Note that from the third layer, our estimative presents better results when compared with Zhang and Ulrych (2002)' method (see Table 3.1).
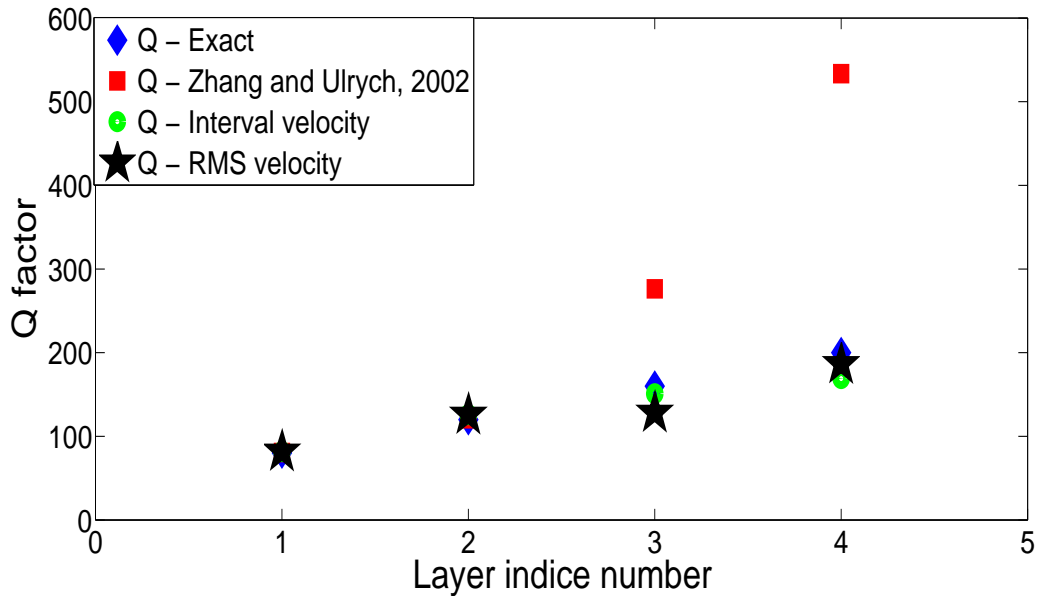
Source: From author

Figure 3.18 – Q factor estimated with redatumed data using the interval velocity and RMS velocity with error of 10%. Note that even with uncertainty in the velocity models, our methodology presented better results (see Table 3.2).
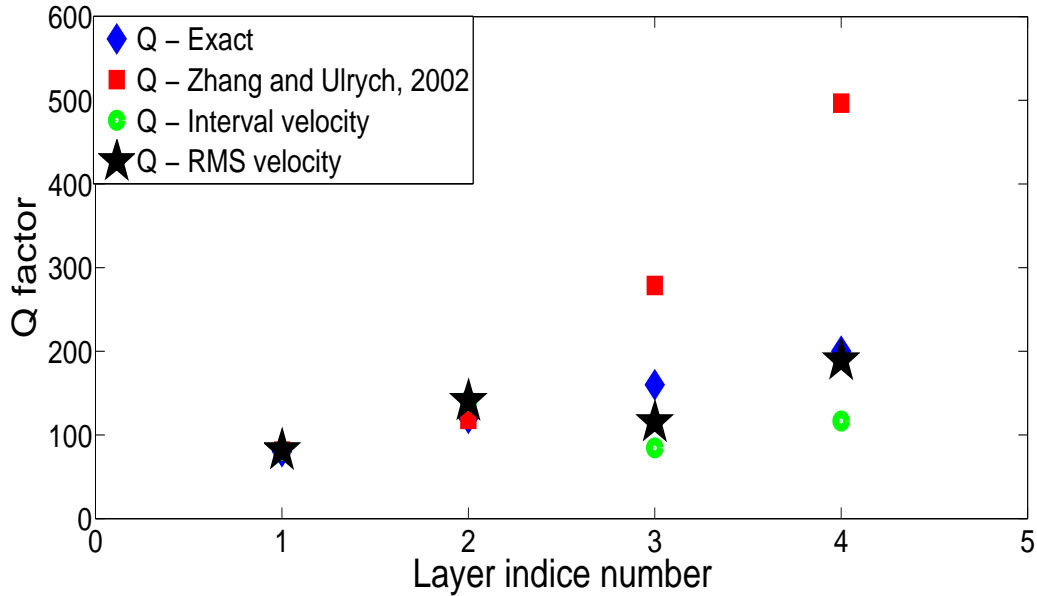
Source: From author

3.3.2 Model II: model with lateral velocity variation

This model has lateral velocity variation, and consists of 5 layers with velocity $v_1 = 2000 \ m/s$, $v_2 = 3162 \ m/s$, $v_3 = 2236 \ m/s$, $v_4 = 3015 \ m/s$ and $v_5 = 3333 \ m/s$. The attenuation factors were $Q_1 = 70$, $Q_2 = 120$, $Q_3 = 50$ and $Q_4 = 160$ (see Figure 3.19). This model also contains a synclinal structure, simulating a gas lens. After modeling, the seismic data was generated and sorted in CDP families.

Figure 3.19 – Synthetic model with lateral velocity variation.
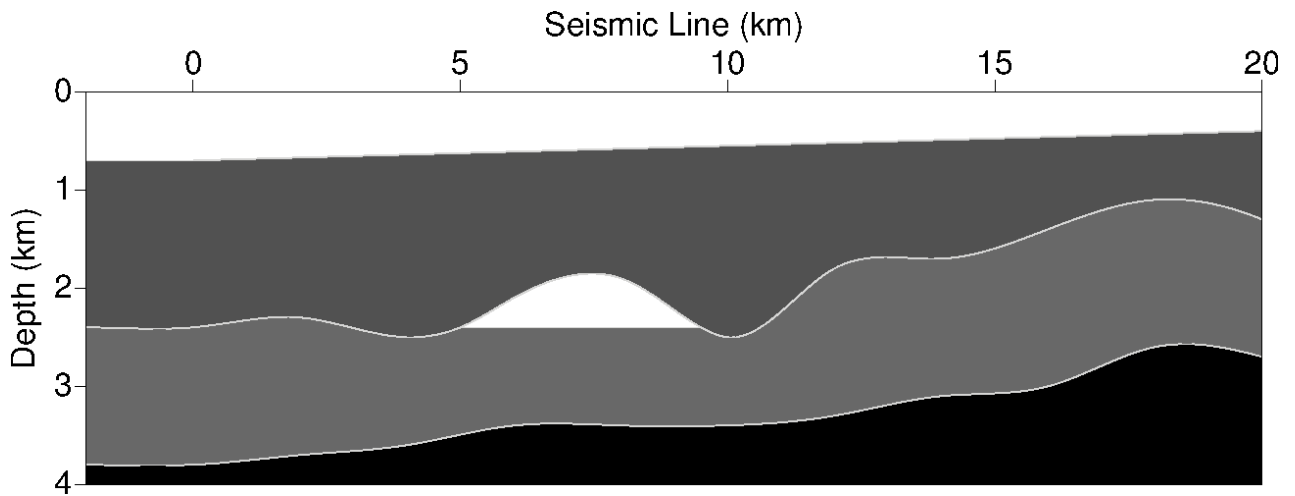
Source: From author

The CDP chosen for our Q-factor estimation was CDP 300 (see Figure 3.20). For this CDP, we recursively performed a redatuming operation to estimate the travel times in each layer. Then, we used the attenuated model to generate the data and the new redatumed time to perform the estimation of the quality factor using the equation (2.32). Figure 3.22 shows the Q-factor values considering the interval velocity and RMS velocity of the layers. It is perceptive that the estimation based on the adapted approach presents better results when compared to the real values of Q. Table 3.3 shows the relative errors of the exact Q values, the values obtained with Zhang's method and the values using the method of this work. As is shown the quality factors estimated by the time correction of the redatuming operator presents better results.

In order to verify the robustness of our method we introduced an error of 10 % in the interval and RMS's velocities. For both velocities, as we can see in Figure 3.23, the estimated quality factor with redatumed data and interval velocity (green point) or RMS velocity (black point) are close to the exact value (blue point), in contrast to the results obtained by the Zhang (in red). We can notice that Zhang estimative shows better approximation to real values (blue point) in the first two layers. However, in the last two layers, the values estimated were far from the true values.

The Q values estimated by our approach were: $Q_1 = 72.3$, $Q_2 = 119.51$, $Q_3 = 48.26$ and $Q_4 = 160.47$ (using RMS velocity). We used these values to perform an inverse Q-filtering operation. This filtering was performed using the compensation filter of PRO-MAX software (Q-filter to amplitude). Figure 3.21 shows the corrected CMP 300. The trace correspondent to position 7.2 km (distance axes) (see Figure 3.19) after correction
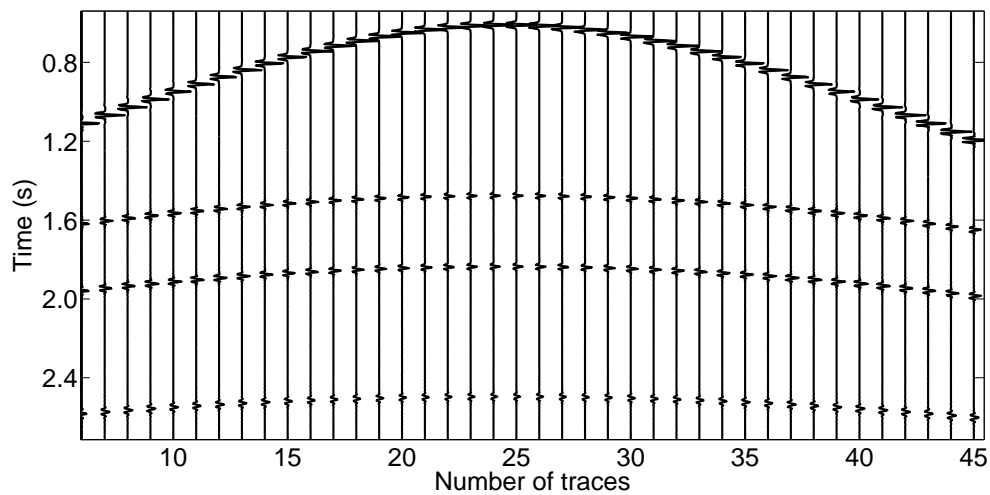
is shown in Figure 3.24. The effect of gas sand in the amplitude signal is quite recovered after Q compensation.

Figure 3.20 – Input attenuated data (CMP 300).
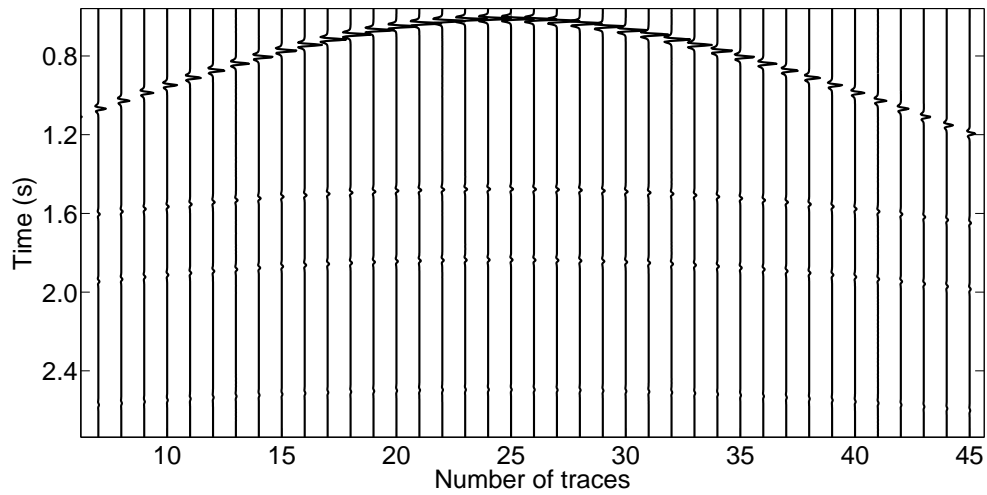
Source: From author

Figure 3.21 – Filtered data with inverse Q filter. The traces in the deeper events present a better amplitude and resolution after compensation.

Source: From author

Table 3.3 – Quality factor estimations. In the first column the exact Q values. In the second the values estimated by Zhang and Ulrych (2002). In the third column the estimative of the quality factors using interval velocity, and in the fourth the estimative using RMS velocity. The others columns show the relative errors of Zhang and Ulrych (2002), PFS with time correction of redatuming using interval velocity and PFS with time correction of redatuming using RMS velocity, respectively

|	Exact	Zhang & Ulrych	Interval vel.	RMS vel.	Error 1	Error 2	Error 3
Q_1	70	72.02	72.02	72.02	2%	2%	2%
Q_2	120	113.16	119.51	119.56	5.8%	0.4%	0.4%
Q_3	50	105.60	48.26	60.15	110%	3.5%	20%
Q_4	160	218.46	160.47	158.58	36%	0.2%	0.8%

Source: From author

Table 3.4 – Quality factor estimated with an error of 10% in the interval velocity and RMS velocity. In the second the values estimated by Zhang and Ulrych (2002). In the third column the estimative of the quality factors using interval velocity, and in the fourth the estimative using RMS velocity. The others columns show the relative erros of Zhang and Ulrych (2002), PFS with time correction of redatuming using interval velocity and PFS with time correction of redatuming using RMS velocity, respectively

	Exact	Zhang and Ulrych	Interval vel.	RMS vel.	Error 1	Error 2	Error 3
Q_1	70	72.02	72.02	72.02	2%	2%	2%
Q_2	120	112.16	121.64	122.53	6.5%	1.3%	2%
Q_3	50	104.61	70.13	66.42	108%	40%	33%
Q_4	160	221.46	152.41	153.51	38%	4.3%	4.0%

Source: From author

Figure 3.22 – Q factor estimated with redatumed data for interval and RMS's velocities. Note that, for the third layer, our estimation present better results when compared to Zhang and Ulrych (2002).
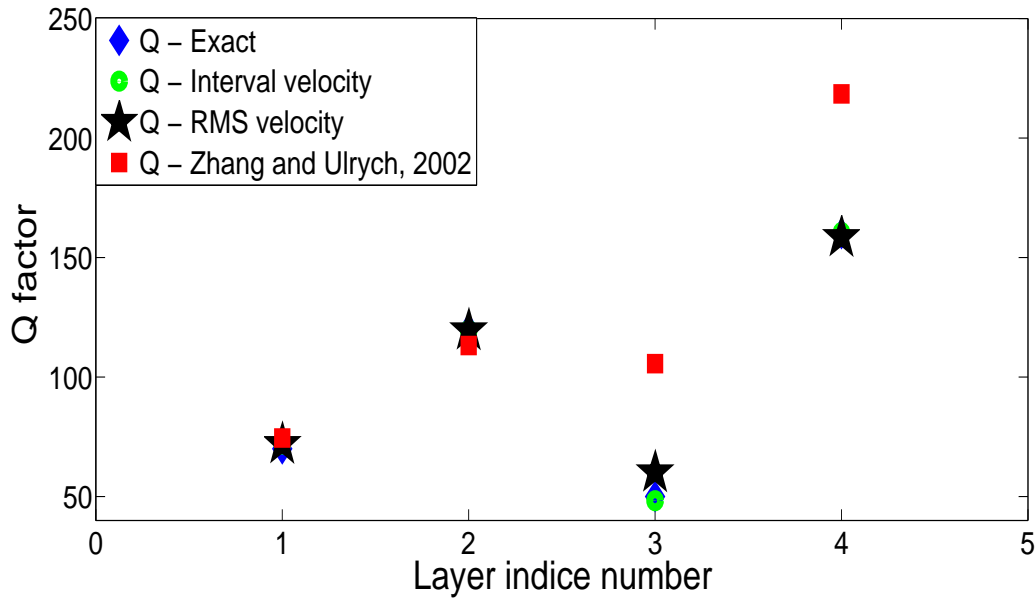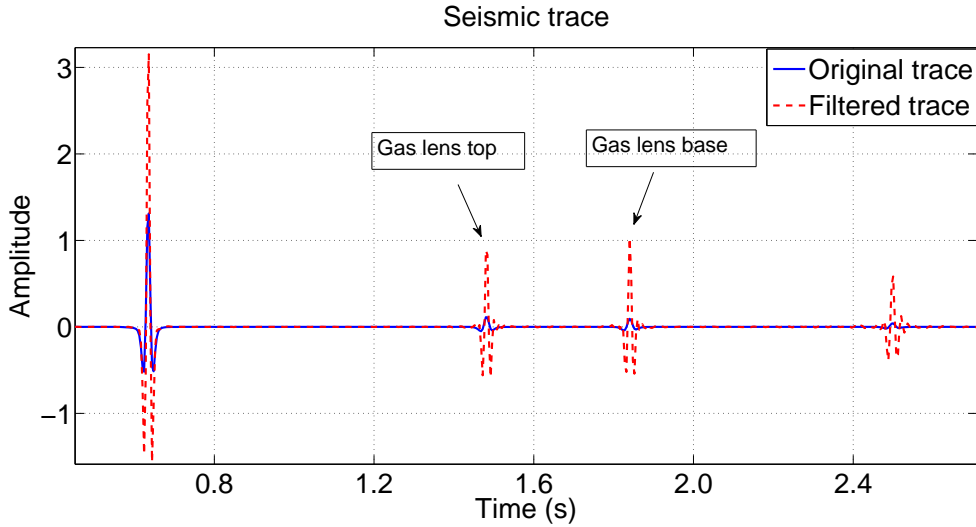

Source: From author

Figure 3.23 – Q factor estimated with redatumed data using the interval and RMS's velocities with an error of 10%. Note that even with this error our methodology presented better results when compared to Zhang and Ulrych (2002).
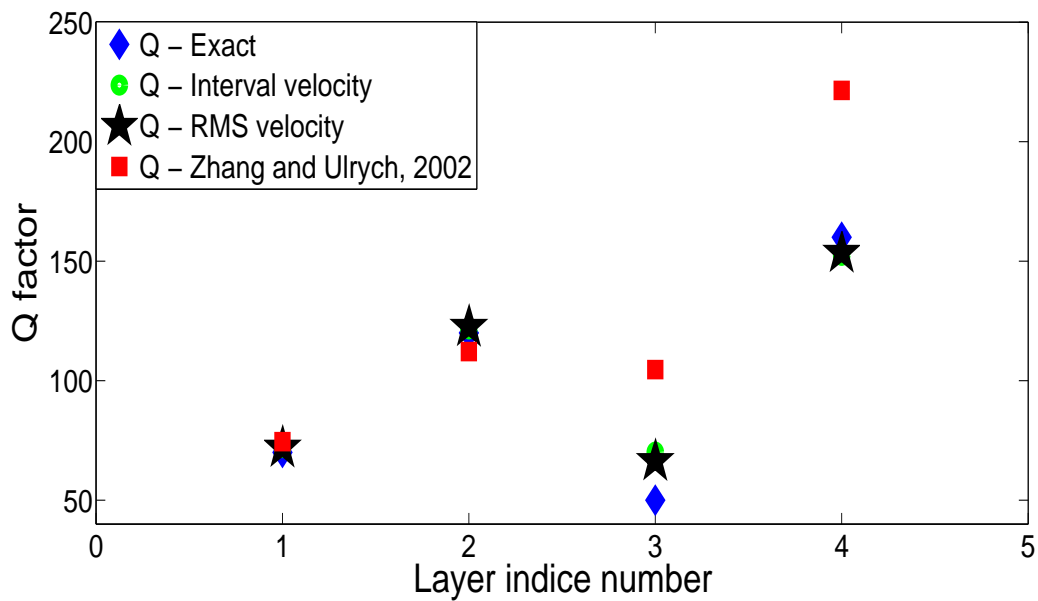
Source: From author

Figure 3.24 – Amplitude of the top and base of gas lens was improved.

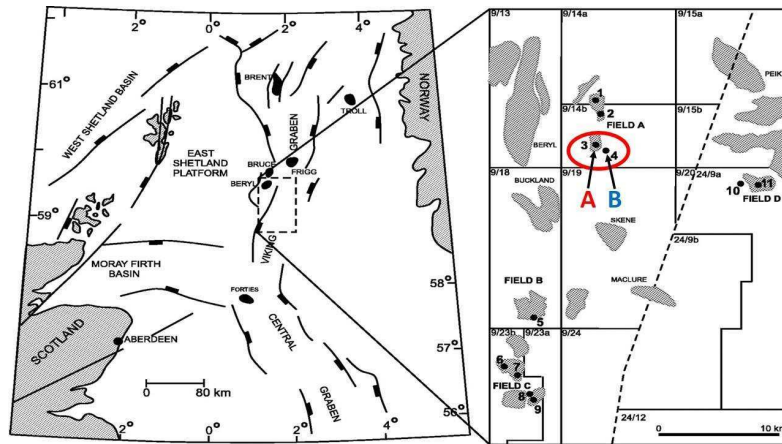Source: From author

3.3.3 Viking graben data set

In this section, we applied the adopted method to a real data set provided by Exxon Mobil (a Viking Graben dataset from the North Sea Basin, see Figure 3.25). The Viking Graben data set was acquired with 1001 shot points and 120 channels. The sampling rate was 4 ms and the recording time was 6 s. The shot interval was 25 m, and 25 m between receivers. The minimum and maximum offsets were of 262 and 3237 m, respectively. The water depth along the seismic line was a relatively constant value of 300 m. Information about geology of Viking Graben can be found in Madiba and McMechan (2003).

The methodology was applied in the CDP gathers with a interval of 100 CPM, resulting in 23 columns of Q. These estimated values located in the 23 columns were interpolated (by cubic spline) and a Q map was generated (see Figure 3.26). After that, this Q map was used in the PROMAX software (in stacked data) in order to obtain the Q inverse filtering. With a stacked section corrected by Q-compensation, we performed a Kirchhoff time migration. Figure 3.27 (a) shows the migrated section without Q composition and Figure 3.27 (b) shows the migrated section after amplitude compensation. We observed the improvement of the signal in amplitude and in resolution, specially in the deeper events.

Figures 3.28 (a) and (b) show a part of the same sections shown in Figures 3.27 (a) and (b). However, in the last case, the reduction in the size of the seismic section was performed to show how the resolution and continuity of the events were improved in the migrated seismic section, with the compensation of the quality factor. Figure 3.29 shows the traces before and after the amplitude correction by inverse Q filtering. This trace

correspond to CMP 808, where according to Madiba and McMechan (2003) this trace correspond to a well location (well A). As we can see in Figure 3.29, in the fracture zone (bellow to 2.0 s , see Figure 3.28), the amplitude is quite attenuated. After amplitude correction, the magnitude of signal is increased as well as the resolution of seismic trace.

Figure 3.25 – Viking Graben map.

Source: From Jonk; Hurst; Duranti; Parnell; Mazzini and Fallick (2005), modified from Brown (1990)

Figure 3.26 – Interpolated map of Q-factors of Viking Graben.
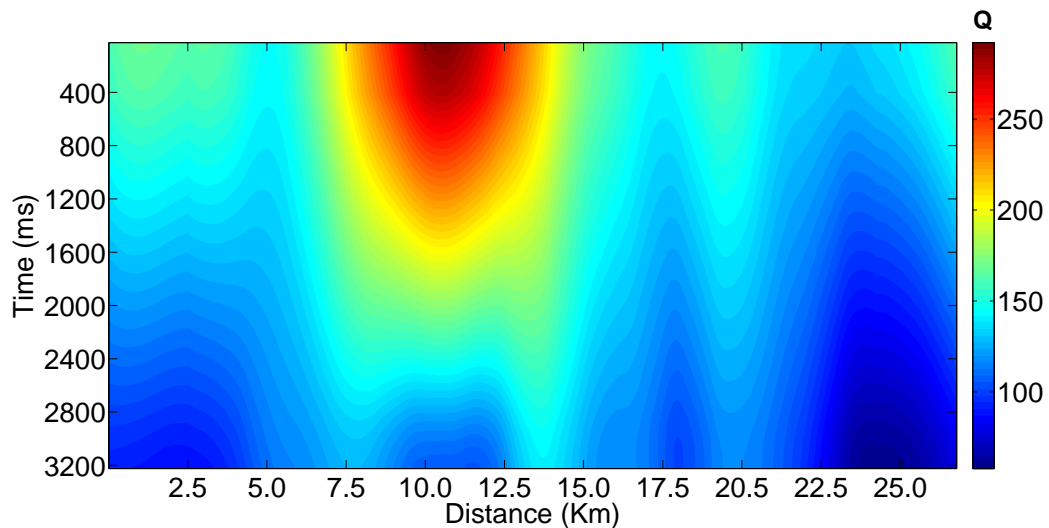
Source: From author

Figure 3.27 – (a) Time migrated section without Q compensation. (b) Time migrated section with Q factor correction. In the last, the deeper events present a better enhancement of amplitude and lateral continuity. Besides, the resolution of the migrated section was considerably increased.

(a)

(b)
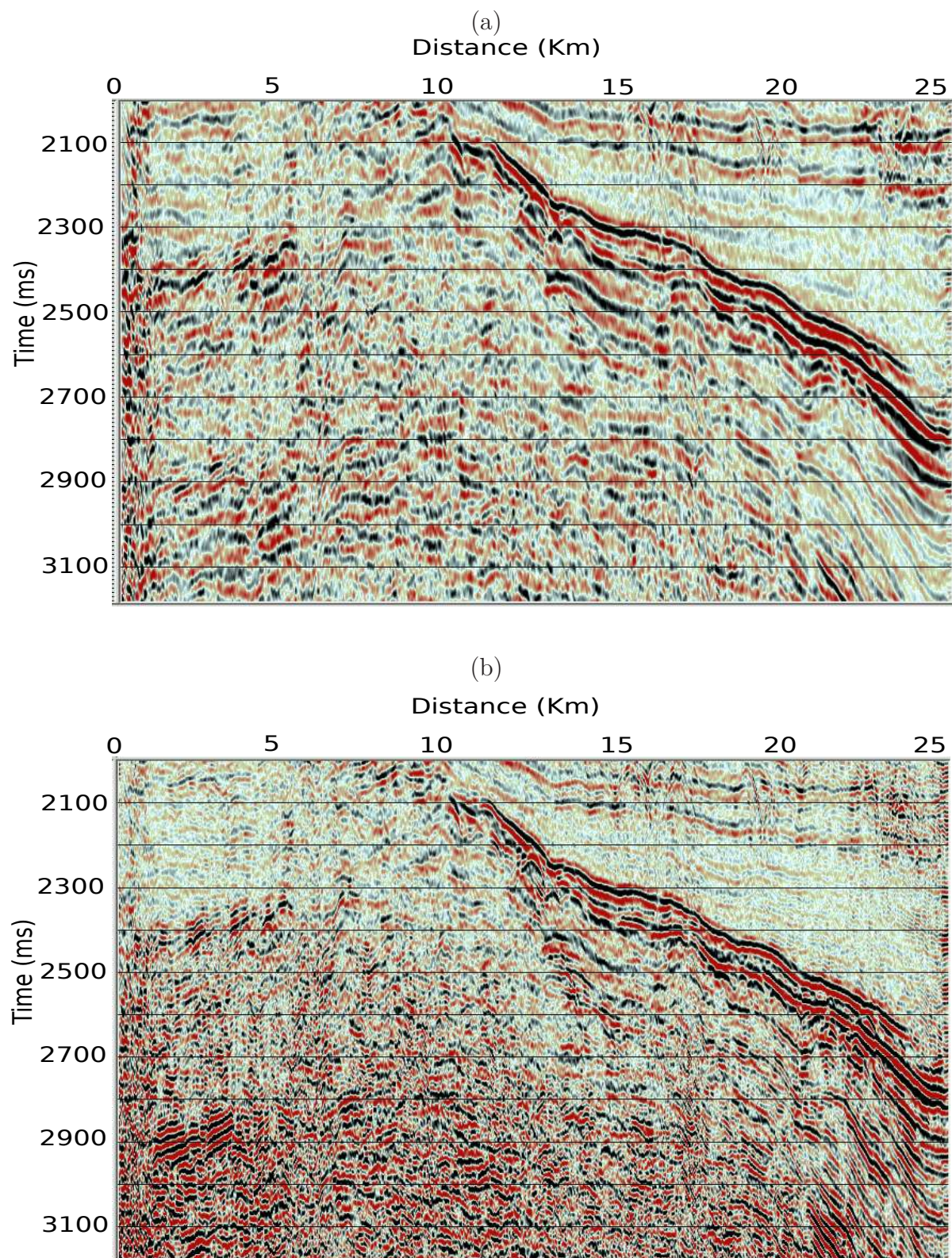
Source: From author

Figure 3.28 – The windowed time migrated sections ((a) without and (b) with Q compensation)
depicted in Figures 3.27 (a) and (b). It is possible to see (with more certainty)
that after Q compensation, the migrated section was considerably improved.

(a)

(b)
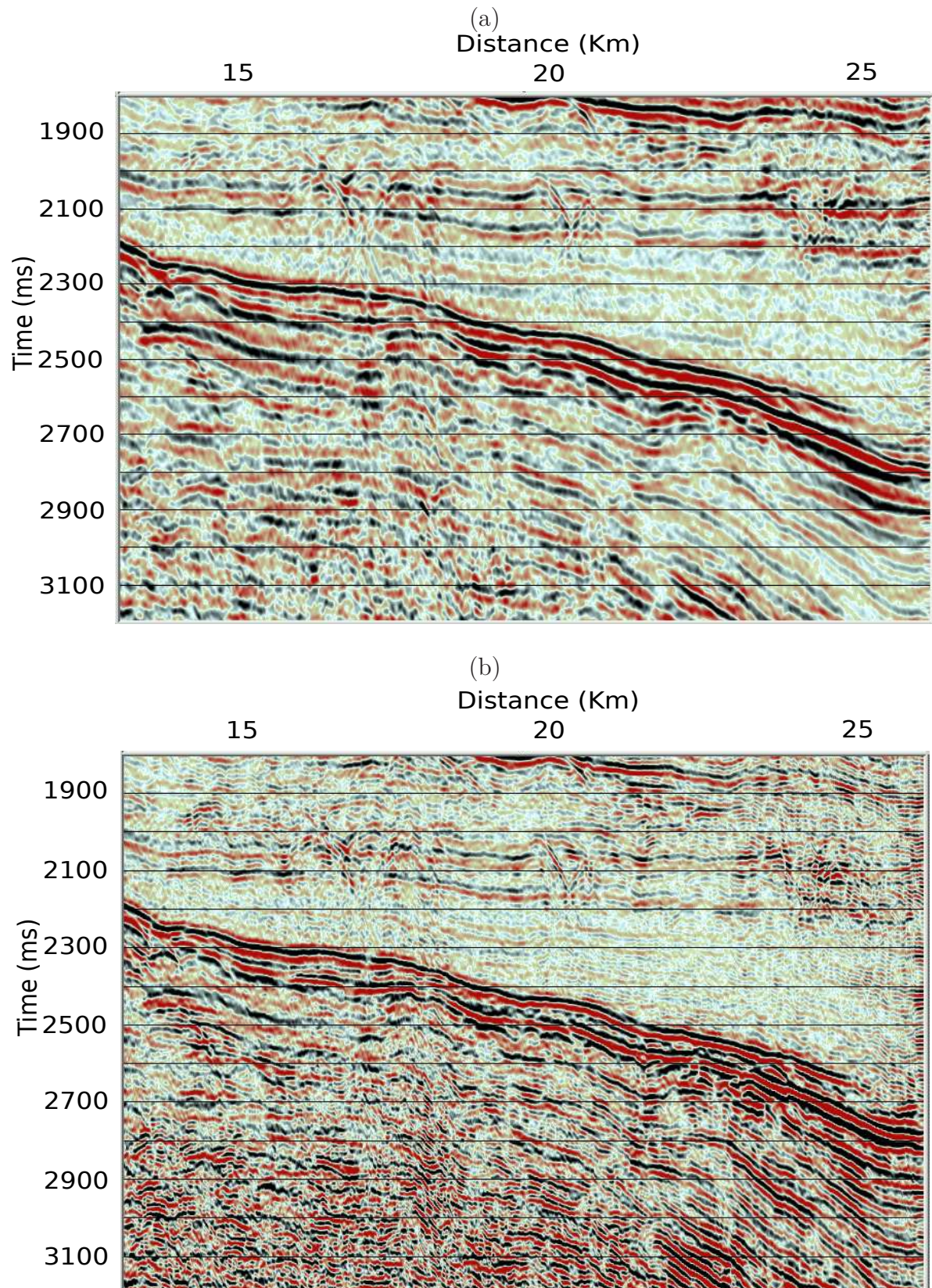
Source: From author

Figure 3.29 – Input seismic trace in blue line and filtered seismic trace in red for CDP 808 for comparison.
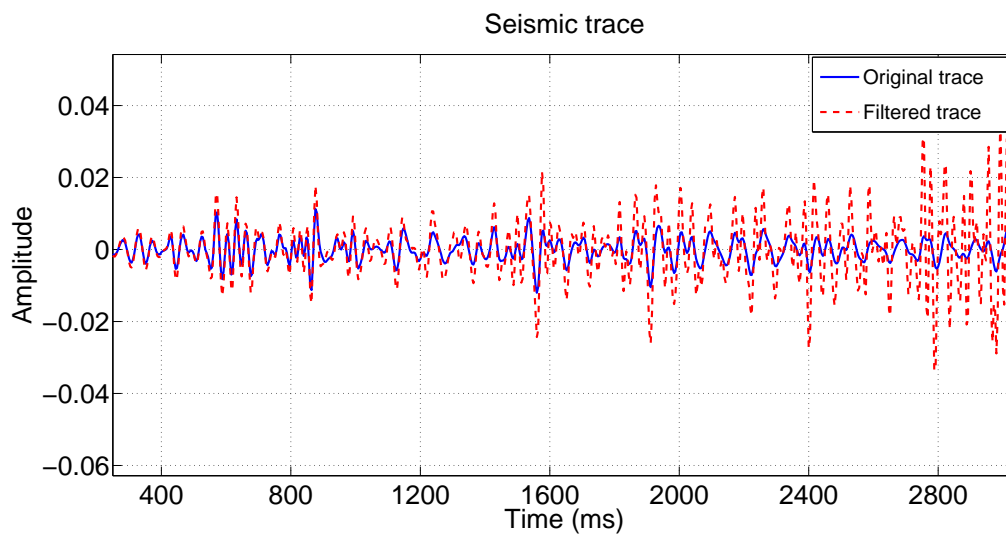
Source: From author

4 CONCLUSIONS

In this work, we performed two analysis. The first one was a comparative analysis on two Kirchhoff redatuming operators: conventional and true-amplitude. The second one, was about joining the redatuming operator (KR) and the frequency shift-method to obtain quality factor value for seismic layered medium.

When formulating both operators as variants of the same Kirchhoff integral operator, it becomes obvious that the difference between them is strictly dynamical, and is due to a geometrical spreading correction factor at the stacking weight. This factor is responsible for replacing the input geometrical spreading by one adjusted to the new measurement surface. The difference is illustrated by numerical examples and one GPR field data set application. Using these examples, we illustrated that both operators fulfill their purposes, either preserving or adjusting the amplitudes. Velocity sensitiveness analysis were also performed both analytically and numerically. We demonstrated that the true-amplitude operator is more sensitive to inaccuracies in the velocity field. While the conventional (amplitude preserving) operator amplitude errors remain low, the true-amplitude operator amplitude errors increase (reaching 27% when in presence of 40% of velocity error).

The feasibility of our results were demonstrated by the application in GPR data of a profile in Siple Dome-Antarctica. The TAKR and KR application to the data showed in both cases, the reflectors were better delineated, presented better lateral continuity and the improved resolution of the main events, specially when the layers were deeper.

After the redatuming operator analysis, we choice the TAKR operator to estimate the quality factor in layered medium. The estimation of the quality factor is view like an important issue for the subsequent filtering of the seismic data. This filtering aims to compensate the attenuation, which is subject to the wave field during propagation, making it possible to obtain a seismic signal with better quality and vertical resolution. In this work, the correction of the rays' traveltime within the layers was extremely important to perform the estimative of the quality factors more precisely. For this purpose, we used the redatuming operator to correct the time propagation in models where the velocity values were approximate (RMS velocity). In the first example (model with plane horizontal layers), using our methodology the quality factor estimation was performed with a highest error of 19.75 % . In the second example (layered model with lateral variation), the highest error in the estimative was around 20 % for a layer. For other layers, the error was about 2 %. Even inducing an error of 10 % in velocity model (RMS and interval) the highest error has not exceeded 40 %.

In general, these numerical examples show the robustness of our methodology when related to errors in velocity. When we applied our methodology in a real data (from Viking Graben), the estimative of Q-factors and then the subsequent inverse Q-filtering, showed how valuable is our methodology to improve the seismic resolution as well as to increase the signal-ratio of amplitude in deep areas significantly affected by fracturing, which is the case of the Viking Graben in the North Sea region. In other words, we can observe an improvement in the deep seismic signal, with a better vertical resolution, amplitude and lateral continuity in the events.

Bibliography

ALKHALIFAH, T.; BAGAINI, C. Straight-rays redatuming: A fast and robust alternative to wave-equation-based datuming. *Geophysics*, v. 71, p. U37–U46, 2006.

ALLEY, R.; BENTLEY., C. Ice-core analysis on the siple coast of west antarctica. *Ann. Glaciol.*, v. 11, p. 1–7, 1988.

BATH, M. *Developments in Solid Earth Geophysics*. [S.l.]: Elsevier Science Publishing Co, 1974.

BERRYHILL, J. R. Wave equation datuming before stack. *Geophysics*, v. 49, p. 2064–2067, 1984.

BEST, A. I.; MCCANN, C.; SOTHCOTT, J. The relationships between the velocities, attenuations and petrophysical properties of reservoir sedimentary rocks. *Geophysical Prospecting*, v. 42, p. 151–178, 1994.

BLEISTEIN, N. *Mathematical Methods for Wave Phenomena*. [S.l.]: Academic Press, New York, 1984.

BLEISTEIN, N. Two-and-one-half dimensional inplane wave propagation. *Geophysical Prospecting*, v. 34, p. 686–703, 1986.

BLIAS, E. Accurate interval Q-factor estimation from VSP data. *Geophysics*, v. 77, n. WA149-WA156, 2012.

BRADFORD, J. *Characterizing shallow aquifers with wave-propagation based geophysical methods: Imaging and attribute analysis*. Tese (Doutorado) — Rice University, Houston, USA, http://hdl.handle.net/1911/18730., 1999.

BROWN, R. J. S. Introduction to the petroleum geology of the north sea. *Special Publication Geological Society*, v. 61, p. 219–254,, 1990.

BRZOSTOWSKI, M. A.; MCMECHAN, G. A. 3-d tomographic imaging of near-surface seismic velocity and attenuatio. *Geophysics*, v. 57, p. 396–403, 1992.

CARCIONE, J. M.; HELLE, H. B.; PHAM, N. H. White's model for wave propagation in partially satured rocks: Comparaison with poroelastic numerical experiments. *Geophysics*, v. 68, p. 1389–1398, 2003.

CARCIONE, J. M.; PICOTTI, S. P-wave seismic attenuation by slow wave diffusion: Effects of inhomogeneous rock properties. *Geophysics*, v. 71, p. 1–8, 2006.

CASSIDY, N. Evaluating lnapl contamination using gpr signal attenuation analysis and dielectric property measurements: Practical implications for hydrological studies. *J. Contam. Hydrol.*, v. 94, n. 1-2, p. 49–75, DOI:10.1016/j.jconhyd.2007.05.002, 2007.

CATANIA, G.; HULBE, C.; CONWAY, H. Grounding-line basal melt rates determined using radar-derived internal stratigraphy. *Journal of Glaciology*, v. 56, p. 545–554, 2010.

COX, M.; SCHERRER, E.; CHEN, R. *Static corrections for seismic reflection surveys.* [S.l.]: Geophysical References, 1999.

DAN, C. J. et al. Application of Kirchhoff integral wave field extrapolation to water layer datuming for obc record. *Journal of Tropical Oceanography*, v. 30, p. 84–89, 2011.

DASGUPTA, R.; CLARK, R. A. Estimation of Q from surface seismic reflection data. *Geophysics*, v. 63, p. 2120–2128, 1998.

FUTTERMAN, W. I. Dispersive body waves. *Geophysics*, v. 67, p. 279–5291, 1962.

KHWANMUANG, W.; UDPHUAY, S. Ground-penetrating radar attribute analysis for visualization of subsurface archaeological structures. *Leading Edge*, v. 31, n. 8, p. 946–949, DOI: 10.1190/tle31080946.1., 2012.

KLüVER, T. Wavefield separation for dual-sensor data with local handling of aliased energy. In: *SEG Technical Program Expanded Abstracts.* [S.l.: s.n.]. p. 1–5.

KNEIB, G.; SHAPIRO, S. A. Viscoacoustic wave propagatio in 2-d random media and separation of absorption and scattering attenuation. *Geophysics*, v. 56, p. 459–467, 1995.

LIU, L.; LANE, J. W.; QUAN, Y. Radar attenuation tomography using the centroid frequency downshift method. *Journal of Applied Geophysics*, v. 40, p. 105–116, 1998.

MADIBA, G. B.; MCMECHAN, G. A. Processing, inversion, and interpretation of a 2d seismic data set from the North Viking Graben, North Sea. *Geophysics*, v. 68, n. 3, p. 837–848, 2003. ISSN 0016-8033, 1942-2156.

MARGRAVE G., F.; FERGUSON R., J. Wavefield extrapolation by nonstationary phase shift. *Geophysics*, v. 64, p. 1067–1078, 1999.

MÜLLER, T. M.; GUREVICH, B.; LEBEDEV, M. Seismic wave attenuation and dispersion resulting from wave-induced flow in porous rocks - a review. *Geophysics*, v. 75, p. 75A147–75A164, 2010.

NUNES, B. I. D. C. et al. Estimating quality factor from surface seismic data: A comparison of current approaches. *Journal of Applied Geophysics*, v. 75, p. 161–170, 2011.

OLIVEIRA, F. S.; FIGUEIREDO, J. J. S.; FREITAS, L. Redatuming operators analysis in homogeneous media. *ACTA Geophysica*, v. 63, p. 414–431, 2015.

PILA, M. F. et al. True-amplitude single-stack redatuming. *Journal of Applied Geophysics*, v. 105, p. 95–111, 2014.

RICKER, N. The form and laws of propagation of seismic wavelets. *Geophysics*, v. 18, p. 10–40, 1953.

SCHLEICHER, J.; HUBRAL, P.; TYGEL, M. Geometrical-spreading correction by a dual diffraction stack. *Geophysics*, v. 58, n. 12, p. 1870–1873, 1993.

SCHLEICHER, J.; M., T.; HUBRAL, P. *Seismic true-amplitude imaging.* [S.l.]: Tulsa: Society of Exploration Geophysicists, 2007.

SCHMALZ, B.; LENNARTZ, B. Analyses of soil water content variations and gpr attribute distributions. *J. Hydrol*, v. 267, p. 3–4, 217–226, DOI: 10.1016/S0022–1694(02)00152–X., 2002.

SCHNEIDER, W. Integral formulation for kirchhoff migration. *Geophysics*, v. 43, p. 49–76, 1978.

SHERIFF, R. E.; GELDART, L. P. *Exploration Seismology*. 2nd edition. ed. United Kingdom: [s.n.], 1995.

TONN, R. The determination of the seismic quality factor q from vsp data. *Geophysical Prospecting*, v. 39, p. 1–27, 1991.

TYGEL, M. et al. 2.5-d true amplitude kirchhoff migration to zero offset in laterally inhomogeneous media. *Geophysics*, v. 63, p. 557–573, 1998.

URSIN, B. Offsetdependent geometrical spreading in a layered medium. *Geophysics*, v. 55, n. 4, p. 492–496, 1990. ISSN 0016-8033.

WHITE, J. E. Underground sound application of seismic waves. *Elsevier Science Publ*, p. 83–137, 1983.

WIGGINS, J. Attenuation of complex water-bottom multiples by wave-equation-based prediction and subtraction. *Geophysics*, v. 53, p. 1527–1539, 1988.

XU, X.; TSVANKIN, I. Anisotropic geometrical-spreading correction for wide-azimuth P-wave reflections. *Geophysics*, v. 71, n. 5, p. D161–D170, 2006.

XU, X.; TSVANKIN, I. A case study of azimuthal AVO analysis with anisotropic spreading correction. *The Leading Edge*, v. 26, n. 12, p. 1552–1561, 2007. ISSN 1070-485X.

ZHANG, C. *Seismic Absorption Estimation and Compensation*. Tese (Doutorado) — University of British Columbia, 2008.

ZHANG, Z.; ULRYCH, T. J. Estimation of quality factors from cmp records. *Geophysics*, v. 67, p. 1542–1547, 2002.

ZHAO, W. et al. Ground penetrating radar (gpr) attribute analysis for archaeological prospection. *J. Appl. Geophys.*, v. 97, p. 107–117, DOI: 10.1016/j.jappgeo.2013.04.010., 2013.

APPENDIX

APPENDIX A – Fourier Transform Definition

The Fourier Transform Definition

There are several common conventions for defining the Fourier transform $\hat{f}$ of an integrable function f : $\mathbb{R} \to \mathbb{C}$. This thesis will use the following definition:

$$f(x,\omega) \;=\; \int_{-\infty}^{\infty} f(x,t)e^{-i\omega t}dt, \tag{A.1}$$

and

$$f(x,t) \;=\; \frac{1}{2\pi}\int_{-\infty}^{\infty} f(x,\omega)e^{i\omega t}d\omega. \tag{A.2}$$

APPENDIX B – List of Publications

Published expanded abstracts

COLLAZOS, J.; OLIVEIRA, F. S.; DE FIGUEIREDO, J. J. S.; FREITAS, L. Develop of Initial depth velocity model improvement from well logs information: 2D Viking Graben data set application. 6th Brazilian Symposium of Geophysics, 2014.

OLIVEIRA, F. S.; Pila, M. F.; NOVAIS, A.; COSTA, J. C.; SCHLEICHER, J. 2.5D True-amplitude diffraction-stack redatuming: numerical tests. In: 11th International Congress of the Brazilian Geophysical Society; EXPOGEF, 2009.

DE FIGUEIREDO, J. J. S; OLIVEIRA, F.; ESMI, E.; FREITAS, L.; GREEN, S.; NO-VAIS, A.; SCHLEICHER, J. Diffraction imaging point of common-offset gather - GPR data example, 81th Ann. Internat. Mtg. Soc. Expl. Geophysiscist, Expanded Abstracts, 2011.

DE FIGUEIREDO, J. J. S; OLIVEIRA, F.; ESMI, E.; L. FREITAS,; NOVAIS, A.; SCHLEICHER, J. Diffraction imaging based on the diffraction operator, Exp;ed, 73rd EAGE Conference ; Exhibition incorporating SPE EUROPEC, 2011.

DE FIGUEIREDO, J. J. S.; OLIVEIRA, F.; ESMI, E.; FREITAS, L.; GREEN, S.; NO-VAIS, A.; SCHLEICHER, J. Diffraction imaging point of common-offset gather - GPR data example, 12th International Congress of the Brazilian Geophysical, Expaned Abstracts, 2011.

Reports scientific

OLIVEIRA, F. S.; NOVAIS, A.; SCHLEICHER, J.; COSTA, J. C. Velocity Dependence of 2.5 D true-amplitude single stack redauming, 13th Anual WIT Meeting, 2010.

DE FIGUEIREDO, J. J. S.,; SCHLEICHER, J.; OLIVEIRA, F.,; ESMI, E.; FREITAS, L.; NOVAIS, A.; GREEN, S.; SUSSNER, P. Automatic detection ; imaging of diffraction points using pattern recognition, 15th Anual WIT Meeting, 2012.

Articles published in international journals

DE FIGUEIREDO, J. J. S.; OLIVEIRA, F.; ESMI, E.; FREITAS, L.; SCHLEICHER, J.; NOVAIS, A.; SUSSNER, P.; GREEN, S. Automatic detection; imaging of diffraction points using pattern recognition. Geophysical Prospecting, v. 61, p. 368-379, 2013.

OLIVEIRA, F. S.; DE FIGUEIREDO, J.J.S.; FREITAS, L. Redatuming operators analysis in homogeneous media. ACTA Geophysics, 63, 414–431, 2015.

Accepted expaned abstracts

OLIVEIRA, F. S.; DE FIGUEIREDO, J.J.S.; OLIVEIRA, A., Joining quality factor estimation ; redatuming operator to improve seismic resolution. 14th International Congress of the Brazilian Geophysical, Expanded Abstracts, 2015.

DE FIGUEIREDO, J.J.S.; COIMBRA, T.; BARROS, C.; OLIVEIRA, F. S.; KIRCH-HOFF, L., Seismic physical modeling of isotropic media based on the physical similitudes. 14th International Congress of the Brazilian Geophysical, Exp;ed Abstracts, 2015.

OLIVEIRA, F. S.; DE FIGUEIREDO, J.J.S.; OLIVEIRA, A., Quality factor estimation based on the frequency shift method ; redatuming operator: application on real dataset. 85TH Annual Meeting SEG, expanded Abstracts, 2015.

Articles submitted and accepted to international journals

OLIVEIRA, F. S.; DE FIGUEIREDO, J.J.S.; GOMES, A. , Estimation of quality factor based on peak frequency-shift method ; redatuming operator: application in real dataset. Geophysics, submitted in 2015.